Empirical battery degradation modelling

similarities, differences and shortcomings of various models

by

Surya Prasad

to obtain the degree of Master of Science
at the Delft University of Technology,
to be defended publicly on Wednesday October 26, 2022 at 09:30 AM.

Student number:	5228794	
Project duration:	December 1, 2021 – October 26, 2022	
Thesis committee:	dr. ir. G. R. Chandra Mouli,	TU Delft, supervisor
	Prof. dr. ir. P. Bauer,	TU Delft
	dr. ir. J. Cremer,	TU Delft

An electronic version of this thesis is available at http://repository.tudelft.nl/.

TU Delft

Abstract

Renewable energy sources, although they are quickly increasing their share in the energy mix, face a major barrier to more widespread adoption. Energy storage solutions overcome this hurdle, and lithium-ion batteries are at the forefront of this. The need for lithium-ion battery degradation studies arises due to the ever increasing use of these batteries in a wide variety of applications.

There exist a large number of empirical and semi-empirical battery degradation models in literature, however their usage with irregular, real world profiles has not been explored. Moreover, understanding where different models can be used and comparing these models is also an area that has not been looked at.

A real world power profile was created in MATLAB based on the WLTP drive cycle. Simultaneously, each model considered was verified against the experimental data for that same model to make sure model predicted degradation values matched the experimental observations. In three models, the verification procedure revealed errors and inaccuracies that were corrected. Implementing an irregular power profile posed two challenges, first, the stress factors of time and throughput required linearized versions of the model equations to be properly accounted for. Second, the identification of cycles in the irregular power profile is usually done using the rainflow counting algorithm, however, an alternative method is proposed in this study.

The real world power profile was applied to each calendar and cyclic ageing model and it was noted that although the power profile was equalized for each cell based on the model in question, the results were widely differing. In some cases, it was possible to explain the differences but in some cases the differences were not easily explained. Apart from the comparison, each model was individually analyzed to understand how degradation phenomena and stress factors affect the accuracy and use case of a model.

Finally, a toolbox was built in MATLAB to summarize the findings of this study, to help users understand where each model studied is likely to be accurate and useful. It was concluded that empirical and semi-empirical models are highly dependent on the testing conditions of the experimental data they are built on, and there are extremely limited scenarios in which these models are applicable outside these conditions. Moreover, accelerated testing conditions which are often used in the experimental phase usually cover different degradation phenomena than those which occur under regular use cases. With respect to the application of irregular (real-world) power profiles to these models, this study details a unique method used to obtain accurate predictions.

Contents

List of Figures

List of Tables

List of Abbreviations

Abbreviation	Meaning
BESS	Battery Energy Storage System
BEV	Battery Electric Vehicle
CAES	Compressed Air Energy Storage
CL	Conductivity Loss
DoD	Depth-of-discharge
DVA	Differential Voltage Analysis
EV	Electric Vehicle
EOL	End-of-life
FCEV	Fuel Cell Electric Vehicle
FEC	Full Equivalent Cycle
FES	Flywheel Energy Storage
HES	Hydrogen Energy Storage
LAM	Loss of Active Material
LCO	Lithium Cobalt Oxide ($LiCoO_2$)
LFP	Lithium Iron Phosphate ($LiFePO_4$)
LIB	Lithium-ion Battery
LLI	Loss of Lithium Inventory
LMO	Lithium Manganese Oxide ($LiMn_2O_4$)
NCA	Lithium Nickel Cobalt Aluminium Oxide ($LiNi_xCo_yAl_zO_2$)
NMC	Lithium Nickel Manganese Cobalt Oxide ($LiMn_xNi_yCo_zO_2$)
PHS	Pumped Hydroelectric Storage
PV	Photovoltaic

Abbreviation	Meaning
RES	Renewable Energy Sources
SCES	Super Capacitor Energy Storage
SEI	Solid Electrolyte Interphase
SoC	State-of-charge
SoH	State-of-health
WLTP	World harmonized Light-duty vehicles Test Procedure

1 Introduction

1.1. The Need for Energy Storage

Conventional energy sources, primarily oil, coal and natural gas have dominated the energy sector for several decades, however they face their fair share of problems, chief among them being the environmental cost and rapid depletion in the face of ever increasing energy demands. Renewable energy sources (RES) are the solution to this problem [1]. Given that energy production and consumption are key factors in economic growth of a country, one can understand both the scale of the problem posed by conventional energy sources and the massive opportunity RES offer [2].

The question of energy storage systems does not come up when conventional energy sources are considered. Since fossil fuel plants (more specifically, natural gas plants) can raise or lower their production to meet demand almost instantaneously, the requirement for energy storage mechanisms in either excess demand or supply situations is greatly reduced [3]. By their very nature RES such as solar and wind energy are intermittent, therefore energy production from these sources cannot be controlled. This poses a major barrier in their large scale integration to the grid as it makes matching demand and supply virtually impossible. Fortunately, a solution to this problem exists in the form of energy storage. Very simply, energy storage mechanisms capture the excess energy produced under sunny/windy conditions and stores it for use during less favourable weather conditions [4, 5].

Several different energy storage systems exist, for example:

- Battery Energy Storage System (BESS)
- Super Capacitor Energy Storage (SCES)
- Flywheel Energy Storage (FES)
- Thermal Energy Storage (TES)
- Pumped Hydroelectric Storage (PHS)
- Compressed Air Energy Storage (CAES)
- Hydrogen Energy Storage (HES)

There are even more storage solutions that exist, and they can be classified based on the energy and power density, cost, response time, operating conditions, efficiency and lifetime [5].

BESS consists of more than just the battery, it also includes the control and power conditioning systems required for BESS to function smoothly. Delving into the battery section, there are various different technologies within this too, namely, lead-acid batteries, sodium sulphur (NaS) batteries, lithium-ion batteries (LIB), metal air batteries and flow batteries. While lead acid batteries are the longest serving and most mature technology, LIBs are considered by many to be have the most scope for further

development and utilization owing to their high energy densities (Fig. 1.1), high coulombic efficiency and relatively low self discharge [6, 7].

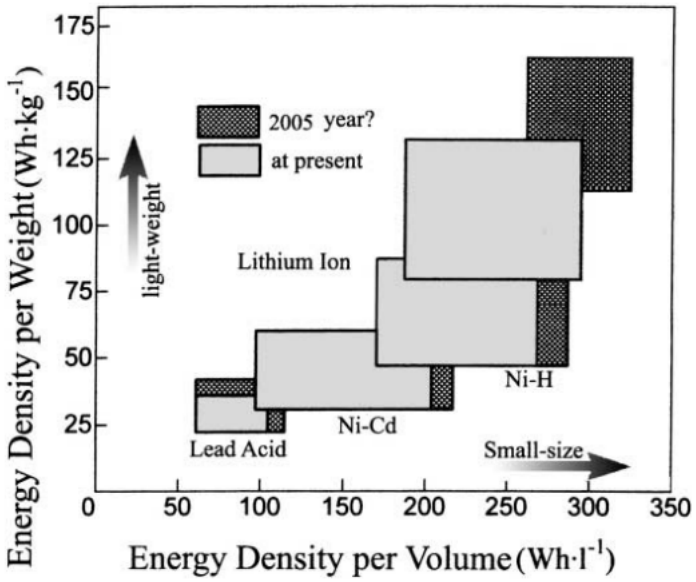

Figure 1.1: Volume and weight energy density comparison for various battery chemistries [8]

1.2. Lithium-ion Batteries

Chemistry	Abbreviation	Chemical Structure
Lithium Cobalt Oxide	LCO	$LiCoO_2$
Lithium Iron Phosphate	LFP	$LiFePO_4$
Lithium Nickel Manganese Cobalt Oxide	NMC	$LiMn_xNi_yCo_zO_2$
Lithium Nickel Cobalt Aluminium Oxide	NCA	$LiNi_xCo_yAl_zO_2$

Table 1.1: Most common LIB cell chemistries [7]

Although LIBs have may have differing chemistries as shown in Table 1.1, the core structure of the battery remains the same and is depicted in Fig. 1.2. The main components of a battery are as follows [9, 10]:

- **Cathode** The cathode is generally made of lithium transition metals with common chemistries mentioned in Table 1.1.
- **Anode** The anode of a LIB is generally made of graphite. Ideally, higher energy and power densities are possible with lithium anodes, but these are subject to high levels of degradation under battery cycling. Other anode materials include Lithium Titanate Oxide ($Li_4Ti_5O_{12}$) or silicon.
- **Electrolyte** The electrolyte is the medium through which ion transport occurs in an LIB. The use case of the electrolyte demands certain features such as a wide operating temperature range, chemical stability with the electrode components, safety and economy.
- **Separator** The separator is a material placed between the two electrodes to prevent contact between them and therefore protect the cell from short circuits. Along with this, it must allow for ion transport through the electrolyte and must therefore be porous and relatively thin.

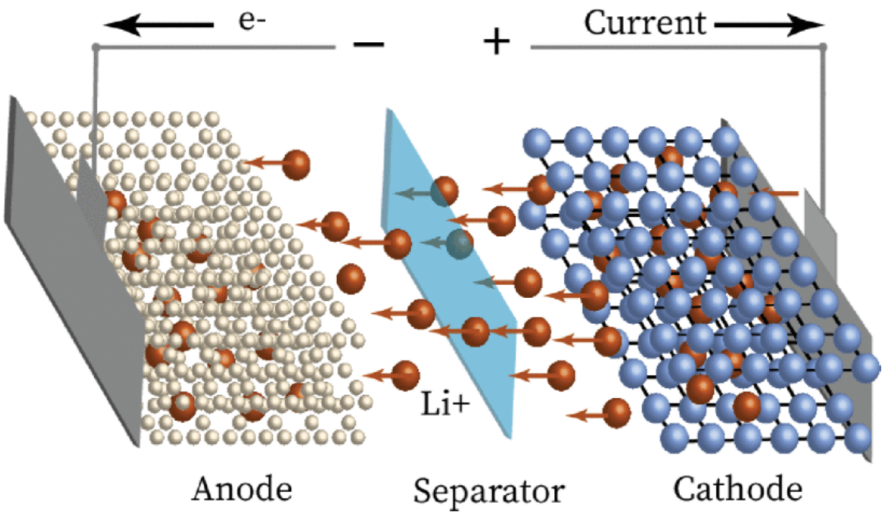

Figure 1.2: Components of a LIB [10]

LIBs are currently used in a variety of applications, as an energy storage system to support increased RES penetration in the grid, in the electrification of the automotive industry as well as widespread use in consumer electronic devices. They are prevalent or show great potential in a number of stationary power grid applications such as grid voltage and frequency regulation and peak shaving as well as supporting decentralized energy generating stations and off-grid photovoltaic (PV) systems [5, 9]. As a solution to the electric mobility question, Battery Electric Vehicles (BEVs) by far outnumber other potential Electric Vehicle (EV) solutions such as Fuel Cell Electric Vehicles (FCEVs).
Given the multitude of current applications and the scope for future use cases, the study of battery degradation is of vital importance. Battery degradation is the loss in capacity and/or increase in resistance of a cell with time and usage. The exact stress factors are discussed in Chapter 2. There are a large number of models available in literature that aim to estimate the state-of-health (SoH) of a battery based on time and usage pattern and these models and the techniques behind them will be discussed in detail in the upcoming chapters.

1.3. Research Goals

The aim of this thesis is to apply different battery degradation models in real world scenarios, understand their accuracy and usability and compare the results obtained from these models with each other. The models are compared to understand the differences in approach, the stress factors considered during modelling, the effect these factors have on the accuracy of results and the scope for further improvement in these models.

The questions considered during the course of this thesis work are as follows:

1. What are the stress factors that effect battery degradation and what effect do they have?
   (a) How do these stress factors affect the mechanisms behind battery degradation?
   (b) What are the different types of models used to depict the effect of these stress factors?
2. How are empirical models applied in real world conditions?
   (a) How can models be verified before they are implemented?
   (b) What challenges do irregular power profiles pose in the implementation of models?

3. How do the testing conditions affect the use case and outputs of different models?
   (a) How can a difference in output for similar test conditions be explained?
   (b) Can models be used outside of their testing conditions and if so, where?
   (c) What are the best use cases for the models studied?
4. Can a user-friendly method to summarize and understand the use cases of models be built and what would its functionality look like?

1.4. Thesis Outline

This study consists of chapters as described below:

- **Chapter 1** which introduces the need for renewables resulting in the need for energy storage, the importance of batteries and lithium-ion batteries within it and therefore the necessity for battery degradation studies
- **Chapter 2** which focuses on battery degradation studies, explaining the degradation mechanisms, the concepts of calendar and cyclic ageing, the stress factors involved and their effect on degradation phenomena and finally the different types of degradation models that exist in literature
- **Chapter 3** which explores a real-world power profile created based on the WLTP drive cycle which is used in later parts of this study to compare the models considered
- **Chapter 4** which details the models being considered, verifies them against the experimental tests conducted in each model, amends models where necessary and introduces a methodology to apply irregular power profiles to these models
- **Chapter 5** which discusses how the degradation phenomena and stress factors described earlier affect the output and use case for each model. This chapter also applies the common power profile to the models studied, attempting to explain the reasons behind the difference in output under identical conditions
- **Chapter 6** which looks back at the research questions detailed in Chapter 1, detailing how, where and to what extent each of these questions have been dealt with along with the future scope based on this study

2

Battery Degradation

Chapter 1 explained the need for renewables, the role of lithium-ion batteries in green energy and the need for battery degradation studies. This chapter looks at the mechanisms occurring in battery degradation, the types of degradation, the stress factors affecting degradation and the various types of battery degradation models that exist in literature.

2.1. Battery Degradation Mechanisms

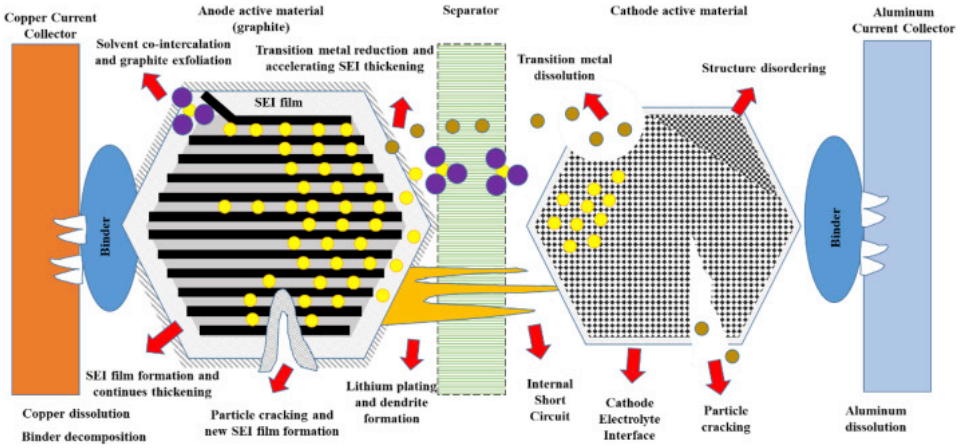

Figure 2.1: Battery degradation mechanisms in LIBs [11]

The main battery degradation mechanisms that occur in LIBs are the following:

- **Loss of Lithium Inventory (LLI)** which occurs when lithium ions are lost in the system as a result of being consumed in parasitic side reactions. These ions are no longer available for cycling between the electrodes and hence represent a loss in capacity. LLI is also caused by lithium ions being trapped in electrically isolated portions of the electrode [12].

- **Loss of Active Material (LAM)** is caused when active sites at the electrodes are no longer available for the intercalation of lithium due to the structural degradation of the electrode (particle cracking, exfoliation or loss of electrical contact) [10, 12].

Sections 2.1.1 & 2.1.2 will delve into the processes occurring at these electrodes that cause a LIB to degrade. Figure 2.1 provides an insight into the different processes taking place in the cell that lead to ageing.

2.1.1. Anode Ageing

Solid Electrolyte Interphase Layer

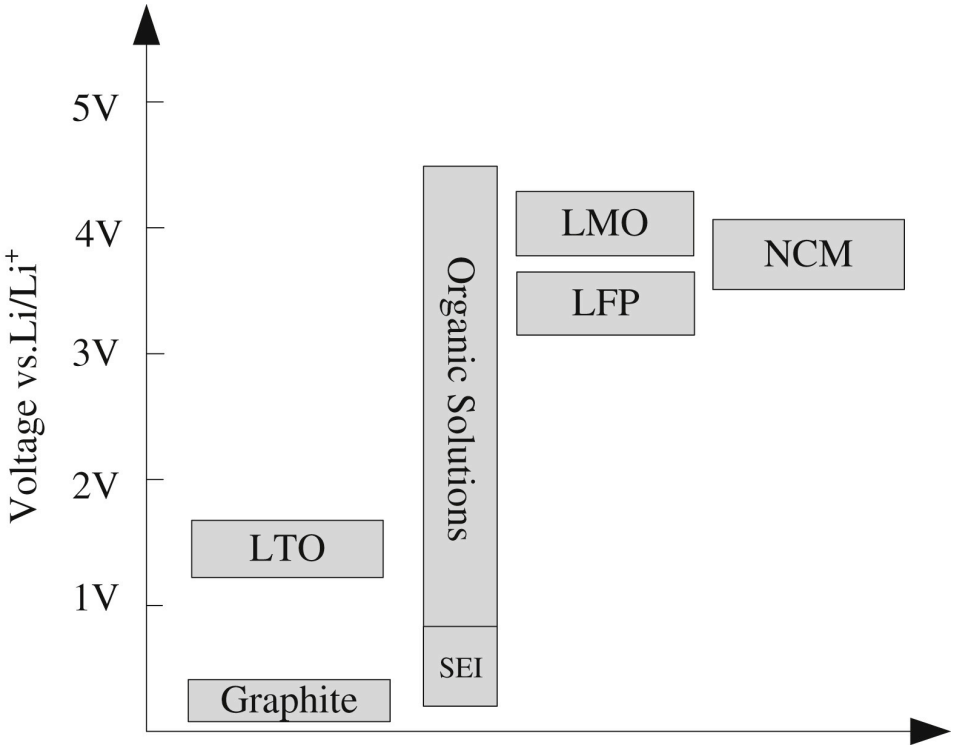

Figure 2.2: Potentials of different electrode chemistries [13]

The most common anode material used in LIBs in graphite. Figure 2.2 shows that voltage window of common electrolytes is between $1 - 4.5V$, while graphite electrodes operate at $0.05V$ meaning that graphite electrodes are generally unstable in regular electrolytes [10, 11, 13]. This causes a reductive decomposition reaction at the electrode-electrolyte interface, consuming lithium ions and forming a passive layer at the surface of the anode called the Solid Electrolyte Interphase (SEI). This phenomenon is especially evident in the first few cycles of a cell, with the SEI formed theoretically being permeable to only lithium ions and protecting the electrode from further contact with the electrolyte [11, 14]. In practice however, the constant intercalation and deintercalaction of lithium ions at the anode causes significant volume changes. This in turn leads to the cracking of the existing SEI, consumption of further lithium inventory and reformation of the SEI [11]. Vetter et al. [15] state that particles apart from lithium ions also appear to diffuse through the SEI as a consequence of which consumption of lithium and electrolyte decomposition occur throughout the lifetime of the battery. This constant generation and growth of the SEI is found to be one of the largest causes of battery ageing. Since the formation of the SEI leads to a loss of cyclable lithium ions, the degradation mechanism involved in the formation of the SEI is LLI.

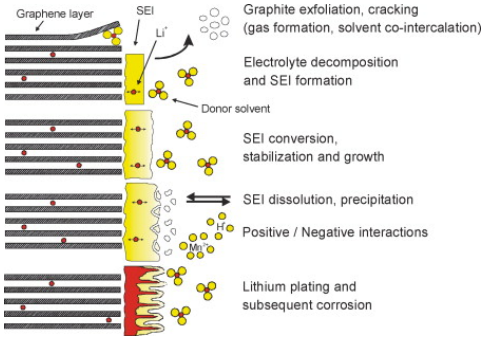

Figure 2.3: Anode ageing process [15]

Lithium Plating

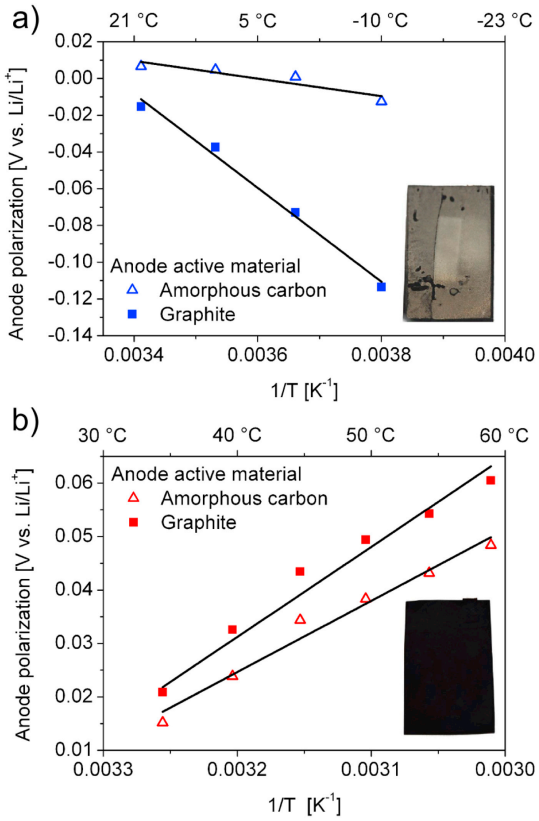

Figure 2.4: Anode polarization at (a) low temperatures and (b) high temperatures [16]

Waldmann et al. [16] state that lithium plating occurring at the anode is a function of anode polarization. They also showed that for both amorphous carbon and graphite electrodes, higher levels of polarization was found at lower temperatures as shown in Fig 2.4. This is in line with [10] & [15] which also state that lithium plating is most likely to occur at low temperatures and high c-rates. The dominant ageing mechanism present in lithium plating is LAM.

Other Ageing Mechanisms

Among the other ageing mechanisms for the anode is mechanical stress caused by the repeated insertion and removal of lithium at the anode. As mentioned before, this process causes volume changes at the anode, leading to cracking of the SEI, exposure of the electrode surface to the electrolyte and further SEI formation. Another ageing process occurs due to the dissolution of transition metals. Transition metals such as iron, cobalt, manganese and nickel dissolve in hydrogen fluoride (HF), which

is present in electrolytes containing lithium hexafluorophosphate ($LiPF_6$). These dissolved transition metals then attach to the anode causing the formation of lithium dendrites, which could lead to internal short circuits [17]. Fig 2.5 schematically explains the entire process. While mechanical stress leading to SEI cracking causes LLI, the dissolution of transition metals leads to LAM.

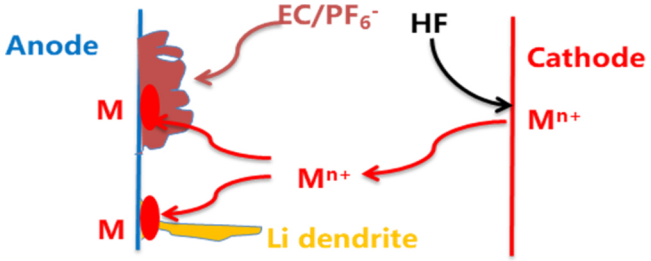

Figure 2.5: Lithium dendrite growth due to transition metal dissolution [17]

2.1.2. Cathode Ageing

Cathode ageing is generally considered less impactful in terms of battery degradation, however, there are a few degradation mechanisms to note:

- Cathode electrolyte interphase: Similar to the SEI formed at the anode, there is a surface film called the Cathode Electrolyte Interphase (CEI) formed on the surface of the cathode. Edstrom et al. [18] note the formation of a *solid permeable interface* formed for a variety of different chemistries studied. The composition of this layer varied for each case.
- Mechanical stress: Just as in the case of the anode, the cathode too undergoes changes in volume during lithium intercalation and deintercalation. The amount of volume change varies based on the chemistry with LFP cells (which have only two phases) showing less volume change than NMC or NCA cells.
- Transition metal dissolution: As already detailed in Section 2.1.1, certain electrolyte chemical compositions react with the transition metals in the cathode, causing them to dissolve in the electrolyte and deposit on the anode surface.

2.2. Calendar Ageing

Battery ageing can be divided into two main sections, calendar ageing and cyclic ageing. Calendar ageing is the irreversible degradation of the battery that occurs when it is not in use. Calendar ageing is widely reported to be dependent on three stress factors; time, temperature and SoC. This section will discuss in detail the impact of each of these stress factors on the ageing process.

2.2.1. Time

The formation of the SEI layer which is the most significant cause of battery degradation in graphite anode based LIBs is generally modelled as a power law relationship with time as shown in Eqn 2.1. The value of z varies between $0.5 - 1$. The most common expression for the effect of time on calendar ageing is a $\sqrt{time}$ relationship.

$$Q_{loss,calendar} \propto t^z \tag{2.1}$$

2.2.2. Temperature

Temperature is one of the most crucial stress factors affecting calendar ageing, and its interdependence with other stress factors also plays an important role. The most common method used to model the temperature effect on calendar ageing is the Arrhenius equation shown in Eqn 2.2 [19, 20].

$$k = B * e^{\frac{-E_a}{RT}} \tag{2.2}$$

where,
$k \rightarrow$ reaction rate

$E_a \rightarrow$ activation energy
$R \rightarrow$ universal gas constant ($= 8.314\ \frac{J}{mol\ K}$)
$T \rightarrow$ temperature

It is commonly reported that increasing temperatures lead to a higher rate of parasitic reactions that form the SEI [15]. Given the general tendency for accelerated ageing tests, i.e., ageing tests conducted at elevated temperatures so as to hasten the ageing process, the relevance of the temperature stress factor especially in terms of its effect on the degradation mechanism and SEI assumes paramount importance. [15, 21, 22] all note that elevated storage temperatures lead to the breakdown of the SEI. This results in the formation of a second SEI of more stable products through the reaction of the electrolyte with intercalated lithium from the anode [22, 23]. The severe effect of elevated temperature storage was highlighted in [22] where a carbon based anode lost less than 1.5% of its capacity when stored for 4 days at $21°C$ but lost around 20% when stored for the same 4 days at $80°C$. Andersson et al. [21] note the formation of a secondary, thicker SEI for graphite electrodes cycled at room temperature before being stored for 7 days above $50°C$. It must be noted that the same thick SEI was not formed for storage temperatures at or below $50°C$, however, the thermal stability of the SEI is a function of not just the chemistry of the electrolyte but also the morphology of the electrode.

2.2.3. SoC

The final stress factor that affects calendar ageing is the SoC (or voltage) of the cell. Although the general trend is that higher SoCs lead to higher levels of degradation, the relationship is a little more nuanced. Most experimental studies conducted with the intention of creating a mathematical degradation model conduct calendar ageing tests under no more than $3-4$ different storage SoCs. Keil et al. [24] demonstrate that calendar ageing does not constantly rise with SoC, instead there are plateau periods of over 20% where the calendar ageing remains fairly constant. Through Differential Voltage Analysis (DVA) the authors of [24] argues that anode potential plays a key role in capacity fade. Low anode potentials (high degree of anode lithiation at high SoC) result in a higher level of capacity fade. The transition from the medium capacity fade plateau to the high capacity fade plateau corresponds well with around 50% degree of lithiation. Low anode potentials which occur at high SoCs (high degree of lithiation) promote electrolytic reduction, resulting in the loss of cyclable lithium and an increased rate of degradation.
[25] & [26] both highlight the detrimental effect the combination of high temperature and high storage SoC has on calendar ageing. It is theorized that the combined effect of a second SEI due to high temperature and a high degree of anode lithiation due to high SoC cause this increased capacity fade.

2.3. Cyclic Ageing

Section 2.2 introduced the first of two types of ageing. This section will discuss cyclic ageing, the degradation of the battery that occurs when a battery is in use, i.e., there is current flowing through it. Cyclic ageing is dependent on certain stress factors, namely throughput, temperature, c-rate, mean SoC and DoD of a cycle.

2.3.1. Throughput

Cell throughput is defined as the total current flowing through a cell over a certain period of time, and is usually measured in Ah. It is analogous to time in calendar ageing. Similar to the case of time in calendar ageing (Section 2.2.1), the effect of throughput on cyclic ageing is generally modelled as a power law relationship as shown in Eqn. 2.3 with the value of z being between $0.5-1$. Cyclic ageing increases with throughput as a result of SEI growth.

$$Q_{loss,cyclic} \propto Ah^z \tag{2.3}$$

2.3.2. Temperature

Just as in the case of calendar ageing, temperature plays an important role in cyclic ageing as well, with the Arrhenius equation (Eqn. 2.2) used to describe the relationship [10, 27]. However, in the case of cyclic ageing, the Arrhenius equation has its limits. Lam and Bauer [28] noted that above temperatures of $25°C$ the degradation followed a particular trend and the Arrhenius equation was valid.

They also noted that below this temperature the modeled capacity fade rate was lower than the actual rate. It was therefore theorized that separate mechanisms were responsible below $25°C$ and above it, rendering the Arrhenius equation unhelpful for temperatures below room temperature. This trend regarding temperature was also noted in [29, 30, 31].
Waldmann et al. [16] noted a similar trend and conducted a post-mortem analysis of an 18650 cell to determine the mechanisms involved in the temperature effect on cyclic ageing. It was concluded that the high temperatures (above $25°C$) lead to an accelerated rate of parasitic side reactions that caused SEI growth and transition metal dissolution, therefore causing increased degradation. It was also found that the mechanism for low temperatures (below $25°C$) was metallic lithium plating. This in turn was attributed to the increased polarization of graphite and amorphous carbon electrodes versus Li/Li^+.

2.3.3. C-rate

The effect of C-rate on the cyclic ageing process is generally found to be interdependent with that of temperature [10]. Maheshwari [32] noted that at room temperature $(20°C)$ the degradation was directly related to C-rate, higher C-rates caused higher levels of degradation, an observation also echoed by [33] & [34]. Generally, high C-rates lead to high current density, this therefore requires faster reactions at the anode for the rapid insertion and de-insertion of lithium ions in the graphite electrode. The mechanical strain caused by this process leads to cracks on the electrode surface causing further SEI formation [32, 34]. At higher temperatures ([32] makes these observations at $45°C$) the requirement for faster diffusion kinetics at high C-rates is compensated by high temperatures, leading to a lower impact of high C-rates.

2.3.4. Mean SoC and DoD

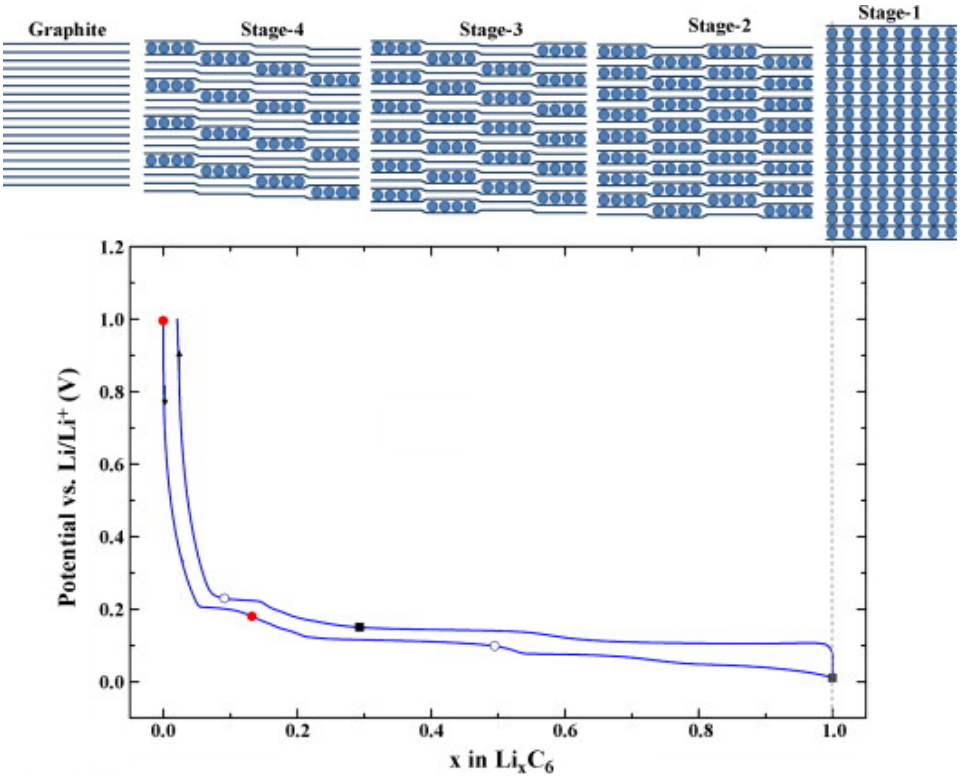

Figure 2.6: Stages of lithium intercalation during the charging process [35]

The effects of mean SoC and DoD are very closely linked to each other, therefore they will be discussed together in this section. Mean SoC and DoD play a crucial role in the intercalation and deintercalaction of lithium at the anode, therefore it is this mechanism and its associated effects that play a major role in battery degradation. Gantenbein et al. [36] and Sethuraman et al. [35] have both looked into this extensively.

[35] states that the concentration of Li^+ ions in the graphite electrodes is greater at the edges than in the bulk, due to the stronger bonds formed between Li^+ ions and edge carbon atoms when compared to between graphene layers. The concentration gradient thus formed between the edge sites and bulk cause local stresses leading to cracking of the SEI and consumption of further active lithium. Moreover, it was also noted that these induced structural stresses are at their highest during the early intercalation phases (stage 3 and 4 in Fig. 2.6, $x < 0.1$ in Li_xC) when compared to more lithium rich phases (stage 1 and 2). [35] therefore concludes that shallow cycling of LIBs at low states of charge, along with repeated discharging of a battery are particularly detrimental to battery longevity.
The approach followed by [36] was different. They hypothesized that the highest degradation would be caused in the conversion of stage 2 to stage 1. They argued that for every twelve layers of graphite, stage 4 would have every fourth layer lithiated, stage 3 would have one extra layer out of twelve being lithiated, stage 2 would have two additional layers out of twelve being lithiated while stage 1 would have six additional layers out of twelve lithiated. Hence, the transition from stage 2 to stage 1 would cause the greatest volume change and through it, the greatest consumption of lithium. This hypothesis was probed by conducting cyclic ageing tests with 20% DoD and across the entire SoC range. The experimental results showed that the highest level of degradation was found during the transition from stage 2 to stage 1, when the cell was cycled between $65 - 85\%$.
It is proposed in this study that both effects detailed above are likely to occur. The lowest SoC range tested in [36] is the range of $5 - 25\%$ SoC, where it shows the least amount of capacity loss. Crucially, tests are not conducted for the cell discharging and charging (0% SoC is not reached) which is potentially why the phenomenon articulated by [35] is not picked up. On, the other hand, [35] conducts long term cyclic ageing experiments for three conditions $Li_{0\leq x<0.1}C$ (cycling between pure graphite and stage 4), $Li_{0.1<x<0.5}C$ (cycling between stage 4 and stage 2) & $Li_{0.3<x\leq 1}C$ (cycling between stage 3 and stage 1) and obtained the maximum degradation in the cycling between a pure graphite and stage 4 composition electrode. Why the effect displayed in [36] is not depicted cannot be clearly explained.

2.4. Modelling of Battery Degradation

Having understood the different mechanisms and stress factors involved in the ageing process, the next natural step is to create models that can accurately depict the lifetime of LIBs taking into account the stress factors and use cases involved. Battery degradation models are generally divided into the following categories:

- **Empirical and semi-empirical models** which are based off data collected from experiments conducted to observe and detail the effects of different stress factors on the ageing process [37, 38]. Mathematical functions like polynomial, exponential and Arrhenius equation (widely used to model the temperature effect) are used to curve fit the relationship of different stress factors in a easy-to-understand, simple manner [39, 40]. The advantages of empirical models stem from their simplicity and ability to provide quick results, with their use being widespread in optimization problems and battery management systems [10]. The downside of empirical models is their poor generality, their effectiveness is restricted to the operating window of the experimental conditions upon which they are built as well as the specific chemistry and cell in question [37, 39, 41]

- **Physical models** also known as electrochemical models aim to model the actual physical mechanisms and processes occurring within a cell (such as the growth of the SEI). The obvious advantage of such models is that the equations provide an insight into the actual degradation mechanisms prevalent and therefore tend to be quite accurate, while their disadvantages are their high computational cost and complexity [39, 41]

- **Equivalent circuit models** on the other hand are not as complex as electrochemical models, and use passive electrical circuitry such as inductors, capacitors and resistors to model cell behaviour. More complicated models may contain one or more RC branches depending on the use case and accuracy required [10, 38, 42]. The advantage of equivalent circuit models is that they are mathematically simple enough to be used in real world scenarios while their disadvantage is that they are dependent on large amounts of test data to be made accurate

Model Type	Advantages	Disadvantages
Empirical Models	Quick computation, simple equations	Lacks generality, narrow operating window
Physical Models	Computationally heavy, complex equations	Accurate, follows degradation mechanisms
Equivalent Circuit Models	Mathematically simple	Require large test matrices to improve accuracy

Table 2.1: Advantages and disadvantages of different modelling techniques

Table 2.1 summarizes the advantages and disadvantages of each modelling technique. Further in this study only empirical and semi-empirical models will be focused on, with details about the implementation method and critical analysis of different models in the ensuing chapters.

2.5. Review of Research Goals

In this chapter, the following aspects of the research goals were addressed:

- The primary degradation mechanisms (LLI and LAM) were understood
- The degradation phenomena (such as the formation of the SEI) were discussed along with the effects each stress factor of calendar and cyclic ageing had on these phenomena
- The different types of degradation models were listed and explained

3

Power Profile

Chapter 1 introduced the motivation for this thesis and research goals, while Chapter 2 detailed the mechanisms, stress factors and various types of models prevalent in the field of battery degradation as well as the current state of literature on these topics. This chapter will focus on how the different empirical and semi-empirical battery degradation models will be compared by detailing a common power profile to be implemented on all models along with scaling the power profile to each specific model based to the cell tested in each case.

3.1. WLTP Power Profile

Every empirical model is created from experimental data for a single cell, meaning the model built from that data can only be used to assess capacity loss (and/or resistance increase) for that particular cell. Since one of the goals of this report is to compare different models, a few common parameters are established to aid this goal. In every case the real world power profile used will be the same (detailed in the following sections) and will be scaled based on the cell being used in each model (detailed in section 3.4).

The real world power profile used in this study is derived from the World harmonized Light-duty vehicles Test Procedure (WLTP) drive cycle for class 3 vehicles (high power vehicles with a power/weight ratio above 34 W/kg). The reference vehicle used was the BMW i3 (120 Ah) whose important specifications are summarized in Table 3.1.

Specification	*Value*
BODY	
Weight (unladen)	$1345kg$
Drag coefficient	0.29
Frontal Area	$2.38m^2$
BATTERY	
Capacity	$42.2kWh$
Energy	$120Ah$
Voltage	$352V$
Cell configuration	$96S1P$
CELL	
Nominal Capacity	$120Ah$
Nominal voltage	$3.6V$

Table 3.1: Relevant specifications for the BMW i3

Figure 3.1 shows the WLTP drive cycle for class 3 vehicles. It contains 4 sections; low, medium, high and extra-high, each with their different top speeds and durations. The sections together constitute

urban, suburban, rural and highway driving scenarios with an almost equal division between urban and rural simulations.

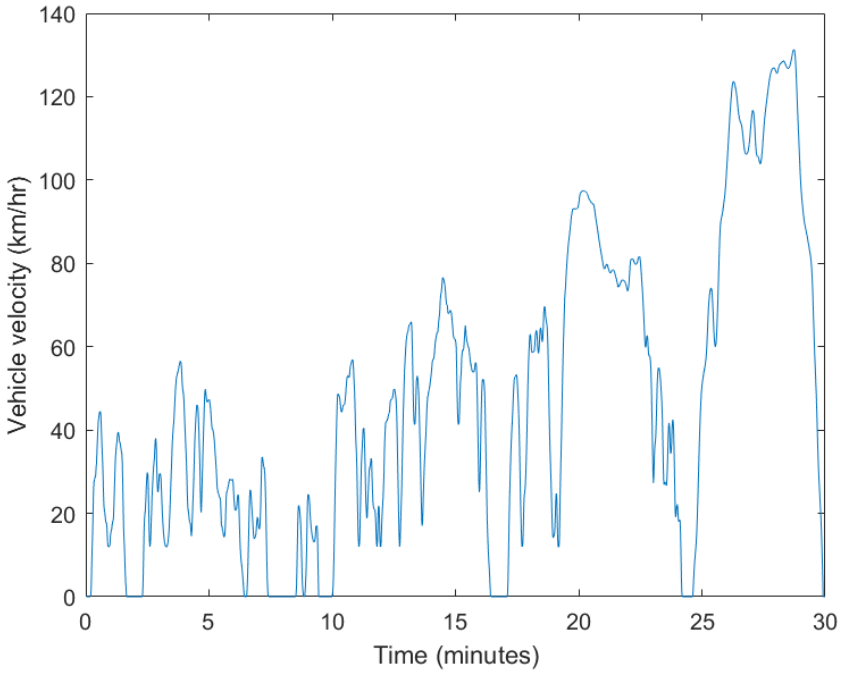

Figure 3.1: Vehicle velocity during WLTP drive cycle

The velocity profile in Figure 3.1 is converted to a power profile by considering the forces acting on a vehicle. These forces can be divided into two types:

- **Resistive forces (F_r):** The resistive forces acting on a vehicle are the aerodynamic drag and rolling resistance. It is assumed that the vehicle is travelling on a level road, therefore gradient force is not considered.
  - Aerodynamic drag (F_d): The aerodynamic drag can be mathematically expressed as shown below.
    $$F_{d_i} = \frac{1}{2} * \rho * c_d * A_f * v_i^2 \tag{3.1}$$
    where,
    $\rho \rightarrow$ density of air ($= 1.225 kg/m^3$)
    $c_d \rightarrow$ drag coefficient (from Table 3.1)
    $A_f \rightarrow$ frontal area of vehicle (from Table 3.1)
    $v \rightarrow$ vehicle velocity in m/s (from Figure 3.1)
  - Rolling resistance (F_{rr}): The rolling resistance can be mathematically expressed as shown below.
    $$F_{rr} = f_r * m * g \tag{3.2}$$
    where,
    $f_r \rightarrow$ coefficient of rolling resistance ($= 0.02$)
    $m \rightarrow$ mass of vehicle (from Table 3.1)
    $g \rightarrow$ acceleration due to gravity ($= 9.81 m/s^2$)
- **Accelerative force (F_a):** The accelerate force is a result of the change in velocity per unit time and can be mathematically expressed as shown below.
  $$F_{a_i} = \frac{v_i - v_{i-1}}{t_i - t_{i-1}} \tag{3.3}$$
  where i refers to the timestep in question.

Once the forces acting on the vehicle have been calculated using Equations 3.1, 3.2 & 3.3, the tractive force (F_t) required can be calculated at each timestep. Note that the direction of resistive force does not change since the direction of the vehicle does not change during the drive cycle. The direction of the accelerative force however changes based on whether the vehicle is accelerating or decelerating.

- Accelerating vehicle ($v_i > v_{i-1}$)

$$F_{t_i} = F_{r_i} + F_{a_i} \tag{3.4}$$

- Constant velocity ($v_i = v_{i-1}$)

$$F_{t_i} = F_{r_i} \tag{3.5}$$

- Decelerating vehicle ($v_i < v_{i-1}$)

$$F_{t_i} = F_{r_i} - F_{a_i} \tag{3.6}$$

The final step is to convert the tractive force (F_t) calculated at each timestep using Equations 3.4-3.6 into power. This is achieved using Equation 3.7 shown below.

$$P_i = F_{t_i} * v_i \tag{3.7}$$

Step Number	Description
Step 1	The resistive and accelerative forces acting on the vehicle per timestep are calculated using Equations 3.1-3.3
Step 2	The tractive force per timestep is calculated based on the acceleration of the car using Equations 3.4-3.6
Step 3	The power per timestep is calculated from the tractive force and vehicle velocity using Equation 3.7

Table 3.2: Steps involved in power calculation

Figure 3.2 shows the result of velocity data from the WLTP cycle being converted into a power profile for the BMW i3 with the data present in Table 3.1 using the steps detailed in Table 3.2. It is important to note that the power on the Y-axis of Fig 3.2 is positive when power is drawn from the battery and negative when power is fed to the battery through regenerative braking. The efficiency of the regenerative braking process is taken to be 70%.

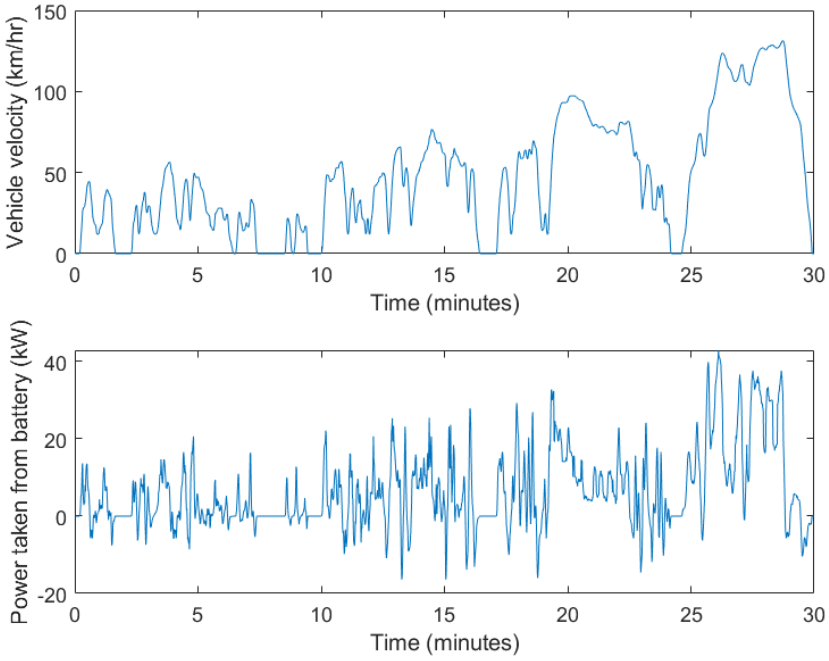

Figure 3.2: Vehicle velocity and power drawn from the battery during WLTP drive cycle

3.2. Derived Parameters

The power profile shown in Fig 3.2 allowed for the calculation of other essential parameters. These parameters were crucial for the mathematical models mentioned in Table 4.1 and will form the basis for the degradation calculations detailed in the forthcoming sections.

Current was calculated by dividing the per timestep power values obtained in Section 3.1 by the battery voltage mentioned in Table 3.1. The current drawn from the battery is shown in Fig 3.3a. It should be noted that just as in the case of Fig 3.2, positive currents denote current drawn from the battery and negative currents denote current fed to the battery.

Distance travelled by the vehicle was calculated as the summation of the velocity over time (with the appropriate units) for each timestep over the entire duration of the drive cycle. The distance travelled by the vehicle is shown in Fig 3.3b. The total distance covered over the drive cycle is $\approx 23km$

Cell throughput is the total energy that has flowed through the cell over the drive cycle period and is measured in ampere hours (Ah). It was calculated as the summation of the absolute value of cell current over time for each timestep over the entire duration of the drive cycle. In this case the battery current and cell current are the same since the configuration of the BMW i3 battery pack (Table 3.1) has all cells in series. The cell throughput is shown in Fig 3.3c.

C-rate measures how quickly a cell is being charged or discharged and was calculated as the ratio of the absolute value of cell current and cell capacity (in Ah). The C-rate is shown in Fig 3.3d.

SoC is calculated using the coulomb counting method where the current at every timestep was integrated over time to obtain the remaining capacity of the cell. The SoC is shown in Fig 3.3e. Note that for coulomb counting, the initial SoC has to be known. In the case of Fig 3.3e the initial SoC was set as 50%.

Cell voltage was used in some models as a substitute for SoC. An exponential fitting model was used to convert SoC data points to cell voltage [43]. The cell voltage is shown in Fig 3.3f. Note that the

exponential model at $25°C$ was used.

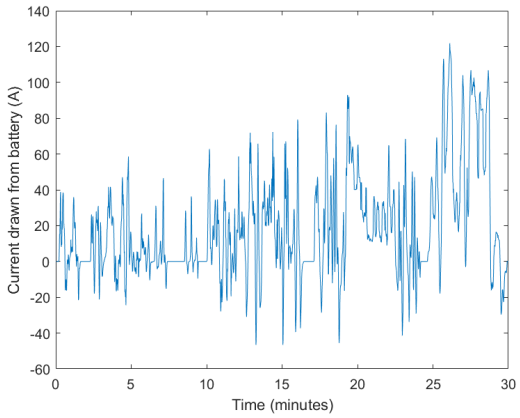

(a) Current drawn from the battery during WLTP drive cycle

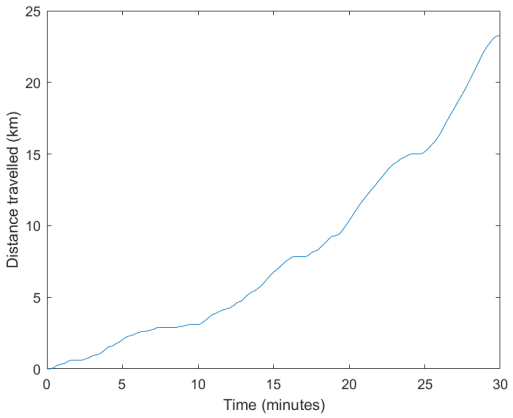

(b) Distance travelled by the vehicle during WLTP drive cycle

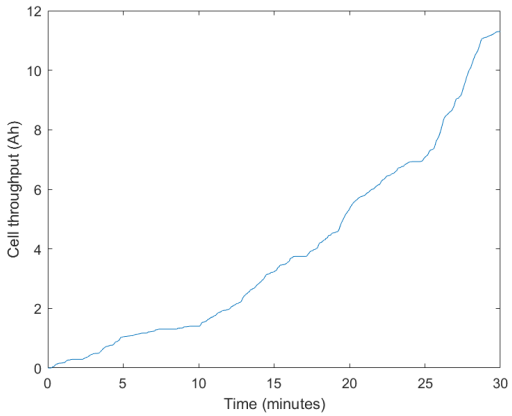

(c) Cell throughput during WLTP drive cycle

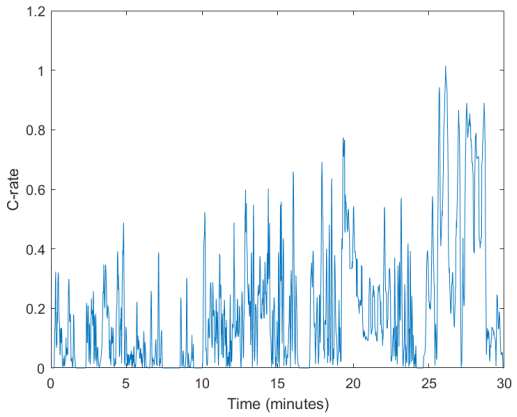

(d) C-rate during WLTP drive cycle

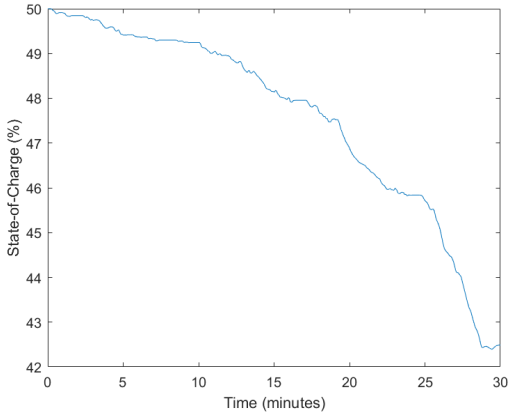

(e) SoC during WLTP drive cycle

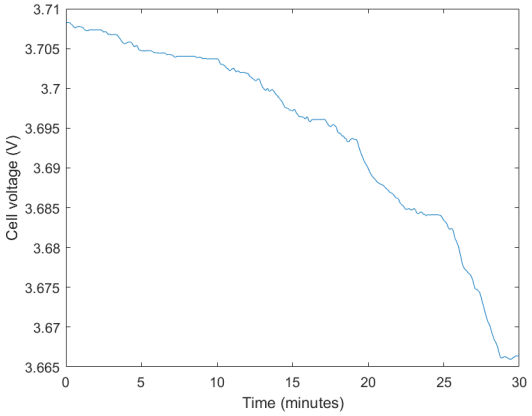

(f) Cell voltage during WLTP drive cycle

Figure 3.3: Parameters derived from power profile of WLTP drive cycle

3.3. Daylong & Yearlong Power Profile

The daylong profile was created based on the WLTP cycle detailed in Section 3.1. A typical daily drive cycle was simulated by combining two WLTP drive cycles and one charging cycle per day, representing a $A \rightarrow B \rightarrow A$ type daily commute followed by charging to a preset maximum SoC at the end of each day. A yearlong power profile was simply created by looping the above-mentioned profile 365 times. Figure 3.4 shows the power profile for a full day.

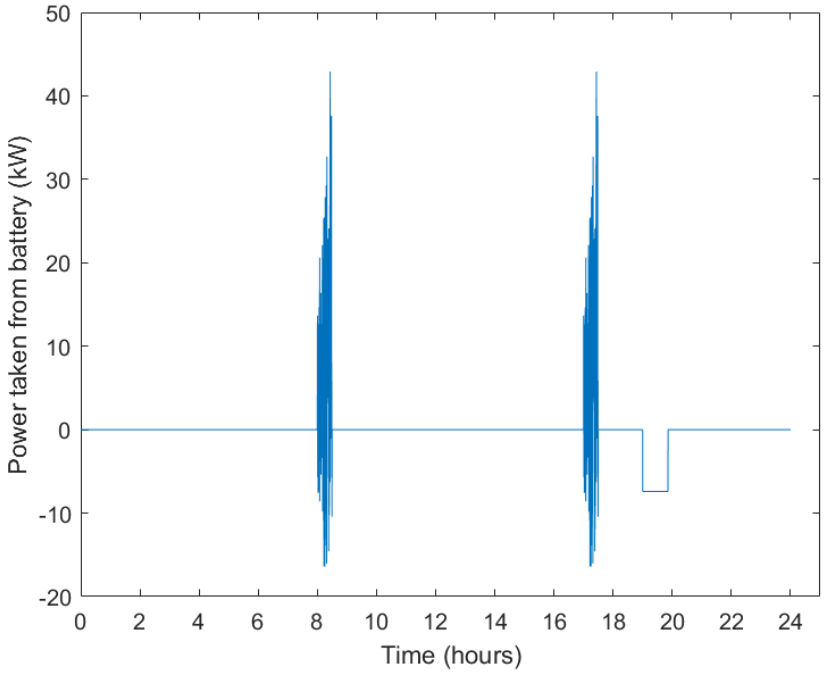

Figure 3.4: Power profile for a full day

3.4. Battery Pack

The reference vehicle for all the modelling presented was a BMW i3 (specifically the BMW i3 with the $120Ah$ battery pack) with a specific cell and a specific configuration used to build the battery pack while each model studied was built to the particular cell used in the experimental section for that model. This presented a problem in the implementation of studied models since the derived parameters shown in Section 3.2 depend on the cell in question.

Battery Source	Cell Specifications	Battery Configuration	Battery Specifications
BMW i3 ($120Ah$)	$3.67V$, $120Ah$	96S, 1P	$42.2kWh$, $120Ah$
[27]	$3.67V$, $2Ah$	96S, 60P	$42.2kWh$, $120Ah$
[44]	$3.67V$, $1.5Ah$	96S, 80P	$42.2kWh$, $120Ah$
[45]	$3.67V$, $5.3Ah$	96S, 22P	$41.0kWh$, $116.6Ah$
[46]	$3.67V$, $3Ah$	96S, 40P	$42.2kWh$, $120Ah$
[47]	$3.67V$, $2.5Ah$	96S, 48P	$42.2kWh$, $120Ah$
[48]	$3.67V$, $3Ah$	96S, 40P	$42.2kWh$, $120Ah$
[49]	$3.67V$, $2.3Ah$	96S, 52P	$42.1kWh$, $119.6Ah$

Table 3.3: Battery configurations for each model

This difficulty was overcome by building a battery pack to the overall specification of the reference battery pack, but out of the cells of the individual models. The BMW i3 has a $42.2kWh$, $120Ah$ battery pack with a specific configuration and the equivalent battery packs for each model along with their configurations are shown in Table 3.3. Through this, the cell current was scaled based on the configuration on the battery pack.

3.5. Review of Research Goals

In this chapter, the following aspects of the research goals were addressed:

- Although this chapter does not deal with the research goals directly, it lays the foundation for a comparison between the different models considered by detailing a common, irregular power profile and the method used to scale it

4

Degradation Modelling

Chapter 2 introduced the primary concepts associated with the study of battery degradation while Chapter 3 detailed the power profile to be used at a later point to compare the models considered in this study. This chapter looks into the specific models under study, their verification as well as the implementation method adopted for irregular power profiles.

4.1. Models Used

The mathematical models used during the modelling process were constrained by the following criteria:

- The cathode chemistry of the reference cell used was restricted to NMC, NMC blends and LFP
- The model type was restricted to empirical/semi-empirical models

Model Number	Reference	Calendar Ageing	Cyclic Ageing	Chemistry
Model 1	[27]	Yes	Yes	NMC
Model 2	[44]	Yes	Yes	NMC-LMO
Model 3	[45]	Yes	No	NMC-LMO
Model 4	[46]	No	Yes*	NMC
Model 5	[47]	Yes	Yes*	LFP
Model 6	[48]	Yes	Yes	LFP
Model 7	[49]	Yes	Yes*	LFP

Table 4.1: Mathematical models used for modelling process in MATLAB

Table 4.1 details the reference papers which the models were extracted from and which types of ageing were investigated. As can be noted, some of the cyclic ageing models have an asterisk next to them. The cyclic ageing data points for these models also contain calendar ageing data, therefore they are not strictly 'pure' cyclic ageing. This will be discussed in greater detail in Section 5.2.1.

4.2. Implementation Method

In each model studied, the experimental conditions applied on the cells can be considered regular. In the case of calendar ageing, the cells were stored at a fixed SoC at a fixed temperature for a fixed amount of time. In the case of cyclic ageing, cells were usually cycled at a fixed c-rate, over a fixed DoD and average voltage. However, the real world power profile detailed in Section 3.3 is irregular, hence the method used to apply the power profile of choice to the models had to be adapted to this use case.

4.2.1. Time and Throughput

Since the power profile being used contains per second power values, the degradation calculations must also be on a per second basis. Two stress factors, time and throughput are unique in that their *cumulative* effect on degradation must always be assessed. This is a particular challenge when considering a discrete power profile with per-second power values. As a result, the degradation needs to be calculated on a per second basis, as the values of different stress factors could change due to the irregular nature of the profile. Regarding the stress factors of time and throughput specifically, the effect of one extra second of calendar ageing is different after 10 seconds (10^{th} to 11^{th} second) when compared to after 100 seconds (100^{th} to 101^{st} second) or after 1000 seconds (1000^{th} to 1001^{st} second); and similarly for throughput. Therefore factoring in the amount of time or throughput *that has already occurred* is of critical importance.

$$f(i) = f(i-1) + \frac{df}{dx}(i-1) * (x(i) - x(i-1)) \tag{4.1}$$

Equation 4.1 is the linearized form of an equation $f(x)$ with respect to x. Taking the equations of model 1 as an example, Eqns 4.7 & 4.8 are the linearized forms of Eqns 4.2 & 4.4 respectively, where i refers to a particular point in time in the case of calendar ageing and a particular cycle in the case of cyclic ageing.

4.2.2. Cycle definition

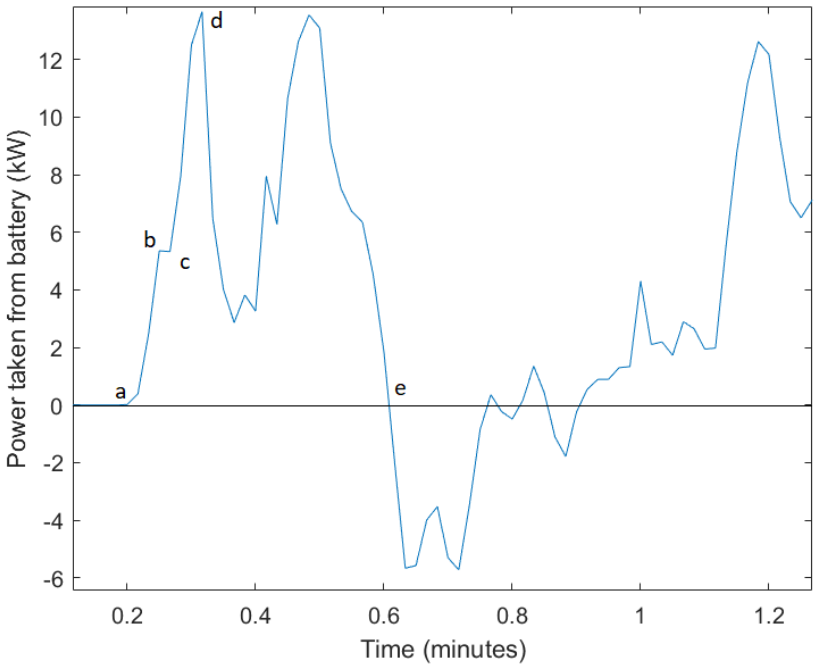

Figure 4.1: WLTP cycle close-up

Cyclic ageing degradation calculations are dependent on how a cycle is defined. During the experimentation phase, cells are subjected to regular cycles with a fixed DoD and c-rate, therefore making the definition of a cycle straightforward. In the case of a irregular power profile as shown in Section 3.3, the definition of a cycle is no longer quite as simple.

Figure 4.1 shows a close-up of a portion of the WLTP power profile discussed in Section 3.1. The first approach used to demarcate cycles was using the rainflow counting algorithm in MATLAB which employs the three-point counting technique [50]. Using this built in function provided cycles such as b-c, a-d and so on (from Fig 4.1). This was not very useful for the purposes of the models studied here, therefore another method where the cycles were marked every time the power curve crossed the

x-axis. In this method, every cycle was either a charge cycle (power values less than zero) or discharge cycle (power values greater than zero). Section a-e in Fig 4.1 shows one such cycle using this method, hereafter called the *zero crossover method*.
Further investigation was done into the use of the rainflow counting algorithm as a cycle counting method. Figure 4.2 illustrates two simple SoC profiles that were used to validate the efficacy of the MATLAB rainflow counting algorithm. The SoC profile in Fig 4.2a shows a cell being charged and discharged between 0-100% in a regular manner. In this case the cycles picked up by the rainflow counting algorithm were a-b, b-c and so on. Figure 4.2b on the other hand shows a SoC profile where the cell is alternatively charged and discharged between 0-100% and 0-50%. Here, the cycles picked up by the rainflow counting algorithm were a-b, c-d, b-e and so on. This counting of cycles makes little physical sense in the current application and is due to the nature of the three-point counting method as explained in [50]. This simple example makes it abundantly clear that although rainflow counting is an often used technique in fatigue analysis, it is not a suitable technique for cycle counting in applications where irregular power or SoC profiles are applied to electrochemical cells.

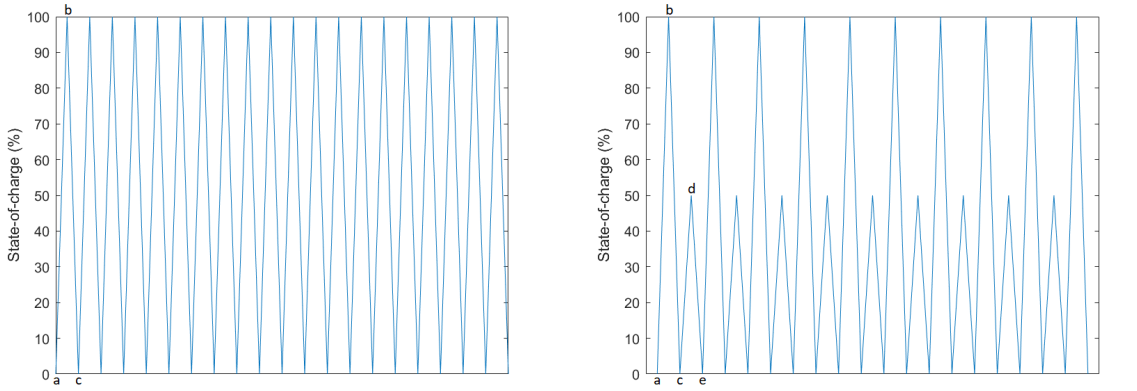

(a) SoC profile consisting of regular 0-100-0% cycles

(b) SoC profile consisting of alternate 0-100-0% & 0-50-0% cycles

Figure 4.2: SoC profile for rainflow counting

4.3. Model 1

Schmalstieg et al. completed a set of accelerated ageing tests on a Sanyo UR18650E cylindrical 18650 type cell and built a an empirical battery degradation model for both capacity loss and resistance increase based on the data collected from the tests [27]. The empirical model presented considered both calendar as well as cyclic ageing.

$$C_{calendar} = 1 - \alpha * t^{0.75} \tag{4.2}$$

$$\alpha = (7.543 * V - 23.75) * 10^6 * e^{\frac{-6976}{T}} \tag{4.3}$$

where,
$V \rightarrow$ cell voltage
$T \rightarrow$ temperature (K)
$t \rightarrow$ time (days)
$C \rightarrow$ ratio of final to initial capacity ($\frac{C_{final}}{C_{initial}}$)

$$C_{cyclic} = 1 - \beta * \sqrt{throughput} \tag{4.4}$$

$$\beta = 7.348 * 10^{-3} * (\bar{V} - 3.667)^2 + 7.600 * 10^{-4} + 4.081 * 10^{-3} * \Delta DoD \tag{4.5}$$

where,
$\bar{V} \rightarrow$ mean cell voltage for a cycle
$\Delta DoD \rightarrow$ DoD for a cycle

$throughput \rightarrow$ cell throughput (Ah)

$$C_{total} = 1 - \alpha * t^{0.75} - \beta * \sqrt{throughput} \tag{4.6}$$

Stress Factor	Range
Calendar Ageing	
Temperature	$35°C$,$40°C$, $50°C$
SoC	0%, 10%, 20%, 30%, 50%, 60%, 70%, 80%, 85%, 90%, 95%
Time	$\approx 500\ days$
Cyclic Ageing	
Depth-of-discharge (DoD)	5%, 10%, 20%, 50%, 80%, 100%
Average SoC	10%, 25%, 50%, 65%, 75%, 80%, 90%, 95%
Throughput	$\approx 4000\ FEC$

Table 4.2: Stress factors and their range for model 1 [27]

Equations 4.2 - 4.6 represent model 1 while Table 4.2 describes the tested range of each stress factor for which experiments were carried out.

Section 4.2 refers to the use of linearized equations to account for the stress factors of time and throughput. Equations 4.7 & 4.8 are the linearized forms of Equations 4.2 & 4.4.

$$C(i) = C(i-1) - \frac{0.75 * \alpha(i-1)}{t^{0.25}} * (t(i) - t(i-1)) \tag{4.7}$$

$$C(i) = C(i-1) - \frac{\beta(i-1)}{2 * \sqrt{Ah}} * (Ah(i) - Ah(i-1)) \tag{4.8}$$

4.3.1. Verification - Model 1

The implementation technique used for model 1 (and every subsequent model) first involved recreating the experimental output values using the model given. The simple objective of this exercise was to establish the accuracy of the model presented. The battery degradation (in the form of capacity loss) was calculated two ways; first as a single calculation of capacity loss after x days and second as a per day linearized calculation of capacity loss after x days. The first method uses Eqn 4.2 or 4.4 (for calendar and cyclic ageing respectively) while the second method uses Eqn 4.7 or 4.8 (for calendar and cyclic ageing respectively) requiring the calculation of the slope of the curve per unit time.

Experimental Conditions	Experimental Result	Model Output	Linearized Model Output
Calendar Ageing			
$500\ days$, $50°C$, $50\%\ SoC$	≈0.82	0.8119	0.8114
$500\ days$, $50°C$, $10\%\ SoC$	≈0.91	0.8751	0.8747
Cyclic Ageing			
$10\%\ DoD$, $50\%\ SoC$, $4000\ FEC$	≈0.92	0.8905	0.8892
$10\%\ DoD$, $25\%\ SoC$, $4000\ FEC$	≈0.86	0.8878	0.8865

Table 4.3: Experiment and model outputs compared for model 1

Table 4.3 compares the experimental results with both types of model outputs for two calendar and two cyclic ageing cases. The outputs shown are the ratio of current capacity (after the experimental period) to initial capacity. In all 4 cases it can be seen that the results from the model are very close to the experimental results, therefore displaying that model 1 was accurate and could be used with the real-life power profile.

4.4. Validation of Implementation Method

Schmalstieg et al. [27] verified their model by creating a verification profile based on a driving profile created through car measurements of a vehicle in Aachen. This profile was then scaled down to a cell level and applied to the cells. This study uses the verification profile considered in [27] to validate the power profile implementation method introduced in Section 4.2.
Figure 4.3 shows the driving profile considered. Three cases were taken into account and are reflected in Fig 4.4, which shows the daylong profile for each case. They are as follows:

- **Case 1** consists of two drive cycles, each of which is followed by a charge cycle where the cell is charged at 1C.
- **Case 2** is similar to the first where it consists of two drive cycles. Prior to each of those drive cycles the cell is charged at 1C.
- **Case 3** consists of repeated drive and charge cycles with very little rest time in between.

For the validation of the implementation technique, the first case described above was considered. A Web Plot Digitizer [51] was used to obtain per second power data which was then converted to a daylong profile similar to case 1 (as shown in Fig 4.4). The daylong profile was looped over for seven months.

The ambient temperature to be considered was provided on a monthly basis. Within each case, three scenarios were considered for three different levels of battery self heating. The first scenario considered no battery heating, the second considered an average increase in temperature due to battery self heating to be $10°C$ and the third scenario considered an average increase in temperature due to battery self heating to be $20°C$.

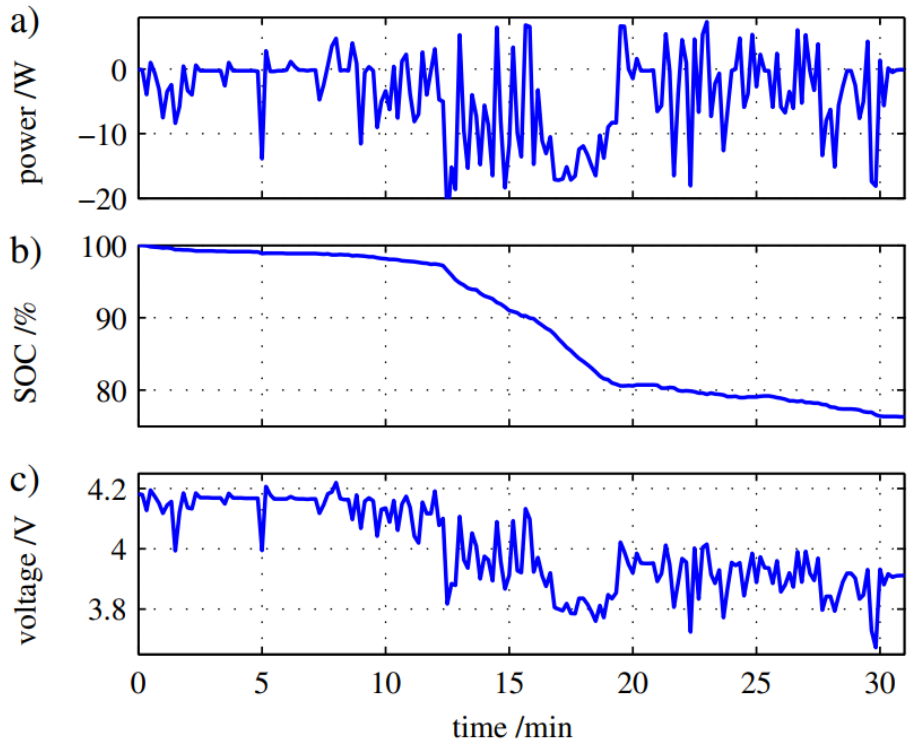

Figure 4.3: Scaled power profile used for validation [27]

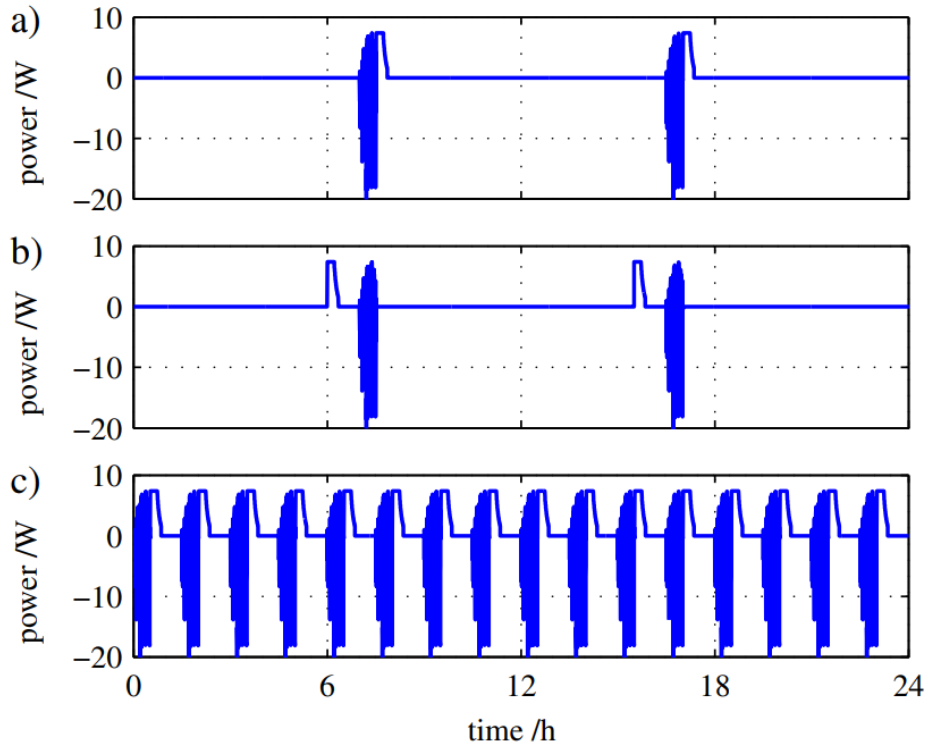

Figure 4.4: Per day power profile based on the drive cycle shown in Fig 4.3 [27]

Table 4.4 compares the experimental test results in [27] with the results of the model using the implementation method described in Section 4.2. The values shown in the table represent the ratio of initial to final capacity ($\frac{C_{initial}}{C_{final}}$). Table 4.4 shows that the model results closely match the experimental results, hence validating the implementation technique adopted.

Scenario	Calendar Ageing Test	Calendar Ageing Model	Total Ageing Test	Total Ageing Model
Ambient temperature	≈ 0.99	0.9914	≈ 0.95	0.9517
Ambient temperature + $10°C$	≈ 0.98	0.9802	≈ 0.94	0.9405
Ambient temperature + $20°C$	≈ 0.97	0.9568	≈ 0.92	0.9171

Table 4.4: Validation of implementation method

4.5. Model 2

Wang et al. investigated the calendar and cyclic ageing of a Sanyo UR18650W graphite/NMC-LMO cell after conducting experiments for a wide range of stress factors [44]. The semi-empirical model presented based on the experimental data is shown below.

Calendar Ageing:

$$Q_{loss,\%} = 14876 * e^{\frac{-24.5*10^3}{RT}} * t^{0.5} \tag{4.9}$$

where,
$R \rightarrow$ universal gas constant ($= 8.314 \frac{J}{molK}$)
$T \rightarrow$ temperature (K)
$t \rightarrow$ time (days)

$Q_{loss,\%}$ → percentage loss in capacity

Cyclic Ageing:

$$Q_{loss,\%} = B_1 * e^{(B_2 * I_{rate})} * throughput \tag{4.10}$$

where,
B_1 = $aT^2 + bT + c$
B_2 = $dT + e$
T → temperature (K)
I_{rate} → c-rate
$throughput$ → cell throughput (Ah)

Total Ageing:

$$Q_{loss,\%} = 14876 * e^{\frac{-24.5*10^3}{RT}} * t^{0.5} + B_1 * e^{(B_2 * I_{rate})} * Ah \tag{4.11}$$

Stress Factor	Range
Cyclic Ageing	
Temperature	$10°C$, $22°C$, $34°C$, $46°C$
Depth-of-discharge (DoD)	50%
C-rate	$0.5C$, $1C$, $2C$, $3.5C$, $5C$, $6.5C$
Throughput	$3000 - 5000\ cycles$

Table 4.5: Stress factors and their range for model 2 [44]

Equations 4.9 - 4.11 represent model 2 while Table 4.5 describes the tested range of each stress factor for which experiments were carried out.

4.5.1. Verification - Model 2

The authors conducted a wide range of experiments under different cyclic ageing conditions, without conducting any specific experiments under calendar ageing conditions. Therefore, the lowest impact cyclic ageing test data ($10°C$, $0.5C$) was used to create the calendar ageing model. It must also be noted that the only stress factors considered for calendar ageing were temperature and time, the SoC of the battery was not considered as a contributing factor. Table 4.6 shows a close match between experimental data and model predictions for both methods of calculation described in 4.3.1. In both Tables 4.6 & 4.7, the values provided are the percentage drop in battery capacity.

Experimental Conditions	Experimental Result	Model Output	Linearized Model Output
$350\ days$, $10°C$	≈9 %	8.4076 %	8.4080 %
$300\ days$, $20°C$	≈10 %	11.9910 %	11.9916 %

Table 4.6: Calendar ageing experiment and model outputs compared for model 2

The comparison between cyclic ageing experimental data and model outputs was carried out in a similar manner to 4.3.1. Therefore, coefficients a-e (Eqn 4.10) were taken as provided by the authors and applied to the model [44]. Column three of Table 4.7 shows the model results using these coefficients and as can be seen, there was a very large gap between the experimental data and model results.
The values for B_1 & B_2 for each of the four temperatures considered in the cyclic ageing experiments was provided by the authors [44]. While B_1 was a second degree polynomial in temperature, B_2 was a first degree polynomial. Using the MATLAB fit function with the given values and temperatures, coefficients a-e were calculated again.
The calculated values using the MATLAB fit function matched those provided by the authors, therefore a larger degree of accuracy (10 decimal places) was used. The difference in model outputs with the higher accuracy coefficients is extremely noticeable and can be seen in column 4 of Table 4.7. The results with higher accuracy coefficients remain close to the experimental data, therefore these coefficients (shown in Table 4.8) were used to implement the yearlong model.

Experimental Conditions	Experimental Result	Low Accuracy Coefficients	High Accuracy Coefficients
$2500\ Ah, 10°C, 0.5C$	≈7.5 %	2.3136 %	6.8549 %
$2500\ Ah, 10°C, 2C$	≈11 %	4.5642 %	13.3698 %

Table 4.7: Cyclic ageing experiment and model outputs for both provided and calculated model 2 coefficients

Coefficient	Low Accuracy Value	High Accuracy Value
a	$8.61 * 10^{-6}$	$8.6124253200 * 10^{-6}$
b	$-5.13 * 10^{-3}$	$-5.1252447196 * 10^{-3}$
c	$7.63 * 10^{-1}$	$7.6291569096 * 10^{-1}$
d	$-6.7 * 10^{-3}$	$-6.7149933066 * 10^{-3}$
e	2.35	2.3467127376

Table 4.8: Low vs high accuracy coefficients for model 2

4.6. Model 3

Baghdadi et al. used data from the SIMCAL project to study and model the degradation of two different battery chemistries NMC/LMO and NCA using Dakin's degradation approach [45, 52]. The generalized form of the formula for a particular parameter (ξ) is shown in Eqn 4.12.

$$\xi(t) = \xi_o * e^{\pm k t^{\alpha}} \tag{4.12}$$

where,
$\xi_o \rightarrow$ initial value of parameter ξ
$k \rightarrow$ degradation rate
$t \rightarrow$ ageing time
$\alpha \rightarrow$ time dependent factor

The stress factors considered and their range of testing is detailed in Table 4.9.

$$k_{calendar} = e^{\frac{c*SoC}{a}} * e^{\frac{d}{a}} * e^{\frac{-b}{aT}} \tag{4.13}$$

where,
$T \rightarrow$ temperature (K)
$SoC \rightarrow$ State-of-Charge

Stress Factor	Range
Calendar Ageing	
Temperature	$30°C, 45°C, 60°C$
SoC	$30\%, 65\%, 100\%$
Time	$500 - 1000\ days$

Table 4.9: Stress factors and their range for model 3 [27]

4.6.1. Verification - Model 3

Equation 4.12 can be rewritten as Eqn 4.14 if ξ is replaced with capacity (C). Equation 4.9 can be rewritten as

$$-ln(\frac{C}{C_o}) = k_{calendar} * t \tag{4.14}$$

Equation 4.13 can be rewritten as 4.15 which is the equation of a flat surface where a, b, c and d are equation parameters.

$$a * ln(k) + \frac{b}{T} - c * SoC - d = 0 \tag{4.15}$$

Just like in the case of the second model, the third model did not provide results matching or close to the experimental data. Columns 2 & 3 of Table 4.10 show that at $30°C$ and 30 % SoC the experimental k value was $9 * 10^{-5}$, the value obtained from the model with the coefficients provided was nowhere close.

Experimental Conditions	**Experimental** $k_{calendar}$	**Model** $k_{calendar}$	**First Degree** $k_{calendar}$	**Second Degree** $k_{calendar}$
$30°C$, 30% SoC	$9 * 10^{-5}$	$1.8133 * 10^{8}$	$5.6571 * 10^{-5}$	$8.0880 * 10^{-5}$
$45°C$, 30% SoC	$30 * 10^{-5}$	$1.8161 * 10^{8}$	$25.979 * 10^{-5}$	$29.396 * 10^{-5}$

Table 4.10: Calendar ageing experiment, model and curve fit outputs for model 3

Since k values for all nine calendar ageing test conditions was provided, two separate surface fits were done. The first surface fit was for a first degree polynomial as shown in 4.16 and the second fit was for a second degree polynomial as shown in 4.17, Through Table 4.10 and Fig 4.5 it is clear that the second degree surface fit provides a closer match to the experimental data.

$$f(x, y) = p_{00} + p_{10}x + p_{01}y \tag{4.16}$$

$$f(x, y) = p_{00} + p_{10}x + p_{01}y + p_{20}x^2 + p_{11}xy + p_{02}y^2 \tag{4.17}$$

Coefficient	**Value**
p_{00}	32.35
p_{10}	9.939
p_{01}	$-1.823 * 10^{4}$
p_{20}	3.785
p_{11}	-3617
p_{02}	$1.71 * 10^{6}$

Table 4.11: Coefficient values for the second degree surface fit of model 3

$$ln(k_{cal}) = p_{00} + p_{10}SoC + \frac{p_{01}}{T} + p_{20}SoC^2 + \frac{p_{11} * SoC}{T} + \frac{p_{02}}{T^2} \tag{4.18}$$

Table 4.11 shows the coefficients of the revised second degree surface fit for model 3 and Eqn 4.18 shows the revised equation for $ln(k_{cal})$ with the same coefficients and stress factors.
Just like in the calendar ageing case, the cyclic ageing output from the model did not match the experimental data. However, the data available in [45] was not enough for an independent curve fit. Therefore, only the calendar ageing portion of this study was used further.

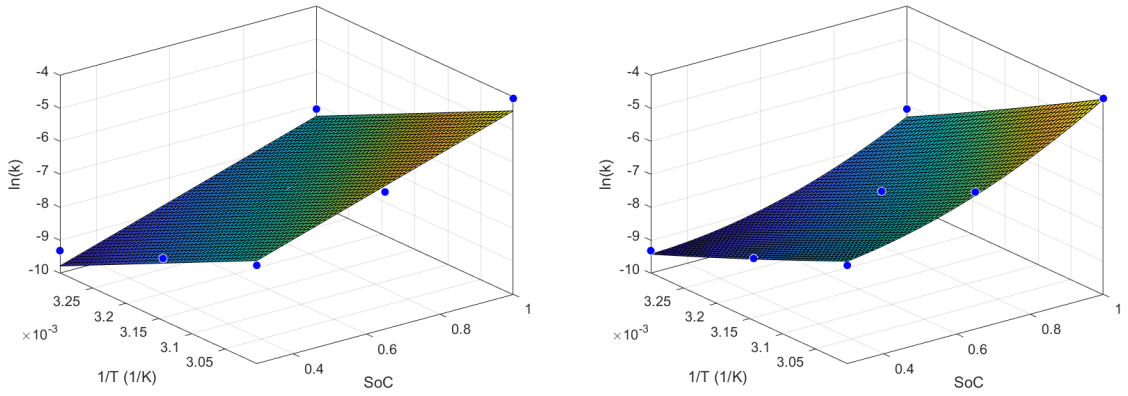

(a) First degree surface fit for model 3 experimental data

(b) Second degree surface fit for model 3 experimental data

Figure 4.5: First and second degree fits for model 3 experimental data

4.7. Model 4

Lee et al. carried out cycle life tests on a $3\ Ah$ pouch type cell with a $LiNi_{0.6}Co_{0.2}Mn_{0.2}O_2$ (NCM622) chemistry [46]. The model subsequently developed from the experimental data was based on the power law relationship similar to Bloom et al. where capacity fade occurs as a power law relation with respect to time, except time was replaced with throughput [46, 53]. Equation 4.19 shows the cyclic ageing model and Table 4.12 shows the stress factors considered in the experiments and their ranges.

$$Q_{loss,\%} = 1.75 * 10^5 * e^{\frac{-E_a}{R*T}} * throughput^{1.317} \tag{4.19}$$

where,
$E_a \rightarrow$ activation energy $(= 4.36 * 10^4\ \frac{J}{mol})$
$R \rightarrow$ gas constant $(= 8.314\ \frac{J}{molK})$
$T \rightarrow$ temperature (K)
$throughput \rightarrow$ cell throughput (Ah)
$Q_{loss,\%} \rightarrow$ percentage loss in capacity

Stress Factor	Range
Cyclic Ageing	
Depth-of-discharge (DoD)	100%
C-rate	$1C$
Temperature	$25°C, 35°C, 45°C$

Table 4.12: Stress factors and their range for model 4 [46]

4.7.1. Verification - Model 4

The model presented was solved both in its original form and its linearized form to see whether it matched the experimental data (as described in Section 4.3.1). Table 4.13 compares the outputs of the model with the experimental data in terms of percentage loss in capacity and it can be clearly seen that the model agrees very closely with the experimental observations.

Experimental Conditions	Experimental Result	Model Output	Linearized Model Output
Cyclic Ageing			
$25°C, 600\ Ah$	$\approx 20\%$	18.3252%	18.3076%
$35°C, 400\ Ah$	$\approx 20\%$	19.0121%	18.9852%

Table 4.13: Experiment and model outputs compared for model 4

4.8. Model 5

Swierczynski et al. studied cells with the $LiFePO_4$ chemistry with a focus on fully electric vehicles [47]. Both calendar and cyclic ageing tests were performed under accelerated conditions with calendar tests performed at high temperatures and cyclic tests performed at high C-rates to simulate EV fast charging. Equations 4.20 & 4.21 constitute the calendar and cyclic capacity fade equations while Table 4.14 shows the stress factors and their ranges.

$$C_{calendar} = (0.019 * SoC^{0.823} + 0.5195) * (3.258 * 10^{-9} * T^{5.087} + 0.295) * t^{0.8} \tag{4.20}$$

where,
$T \rightarrow$ temperature (°C)
$SoC \rightarrow$ State-of-Charge
$t \rightarrow$ time (months)

$$C_{cyclic} = 0.00024 * e^{0.02717*T} * 0.02982 * DoD^{0.4904} * \sqrt{nc} \tag{4.21}$$

where,
$T \rightarrow$ temperature (K)
$DoD \rightarrow$ Depth-of-Discharge
$nc \rightarrow$ number of cycles

Stress Factor	Range
Calendar Ageing	
Temperature	$40°C$, $47°C$, $55°C$
SoC	10%, 50%, 90%
Time	till 80% capacity
Cyclic Ageing	
Depth-of-discharge (DoD)	10%, 45%, 80%
Temperature	$35°C$, $42°C$, $50°C$
Number of cycles	till 80% capacity

Table 4.14: Stress factors and their range for model 5 [47]

4.8.1. Verification - Model 5

The authors defined end-of-life (EOL) as 20% loss in capacity of the cell [47]. Therefore, the calendar and cyclic ageing tests were done to determine the lifetime of the cell as defined. Table 4.15 shows the outputs of the experimental data and model to be the EOL of the cell. As it can be seen, in both the calendar and cyclic ageing cases, model output is very close to the experimental data.

Experimental Conditions	Experimental Result	Model Output	Linearized Model Output
Calendar Ageing			
$40°C$, 50% SoC	20%	19.8999%	19.8713%
$55°C$, 10% SoC	20%	19.9595%	20.0588%
Cyclic Ageing			
$35°C$, 45% DoD	20%	20.0153%	20.0688%
$50°C$, 10% DoD	20%	20.0140%	20.0526%

Table 4.15: Experiment and model outputs compared for model 5

4.9. Model 6

Schimpe et al. created a semi-empirical degradation model for calendar and cyclic ageing based on experimental data of a commercial LFP cell [48]. The unique nature of this model uses internal cell data such as electrode half-cell potential as well as integrating different capacity loss mechanisms. Equation

4.22 is the overall calendar ageing model while Eqns 4.23, 4.24 & 4.25 calculate the parameters of the model.

$$Q_{L,cal}(t) = k_{cal}(T, SoC) * \sqrt{t} \tag{4.22}$$

$$k_{cal}(T, SoC) = k_{cal,ref} * e^{[\frac{-E_{a,cal}}{R}(\frac{1}{T} - \frac{1}{T_{ref}})]} * (e^{[\frac{\alpha * F}{R}(\frac{U_{a,ref} - U_a(SoC)}{T_{ref}})]} + k_0) \tag{4.23}$$

where,
$E_{a,cal}$ → activation energy for calendar ageing
R → universal gas constant ($= 8.314 \frac{J}{molK}$)
T → temperature (K)
T_{ref} → reference temperature ($= 298.15K$)
F → Faraday constant
$U_{a,ref}$ → reference half cell potential
U_a → half-cell potential of the anode
α, k_0 → equation constants
t → time (hours)

$$\begin{aligned} U_a(\chi_a) = 0.6379 + 0.5416 * e^{-305.5309 * \chi_a} + 0.044 tanh(-\frac{\chi_a - 0.1958}{0.1088}) \\ -0.1978 tanh(\frac{\chi_a - 1.0571}{0.0854}) - 0.6875 tanh(\frac{\chi_a + 0.0117}{0.0529}) \\ -0.0175 tanh(\frac{\chi_a - 0.5692}{0.0875}) \end{aligned} \tag{4.24}$$

where,
χ_a → degree of lithiation of the anode

$$\chi_a(SoC) = \chi_a(SoC = 0\%) + SoC * [\chi_a(SoC = 100\%) - \chi_a(SoC = 0\%)] \tag{4.25}$$

Equations 4.26 - 4.29 describe the cyclic ageing degradation model. While Eqns 4.26 & 4.27 define the temperature dependence of cyclic ageing, Eqns 4.28 & 4.29 define the c-rate dependence. Equation 4.30 is the overall cyclic ageing as the summation of Eqns 4.26 & 4.28 while Eqn 4.31 represents the total ageing. Table 4.16 shows the stress factors considered and their respective ranges.

$$Q_{L,cyc,high\,T} = k_{cyc,high\,T}(T) * \sqrt{throughput_{tot}} \tag{4.26}$$

where,
$throughput_{tot}$ → total cell throughput (Ah)

$$k_{cyc,high\,T}(T) = k_{cyc,high\,T,ref} * e^{[\frac{-E_{a,cyc,high\,T}}{R}(\frac{1}{T} - \frac{1}{T_{ref}})]} \tag{4.27}$$

where,
$E_{a,cyc,high\,T}$ → activation energy for cyclic ageing at high temperature
R → universal gas constant ($= 8.314 \frac{J}{molK}$)
T → temperature (K)
T_{ref} → reference temperature ($= 298.15K$)

$$Q_{L,cyc,low\,T} = k_{cyc,low\,T}(T, I_{ch}) * \sqrt{throughput_{ch}} \tag{4.28}$$

where,
$throughput_{tot}$ → charging cell throughput (Ah)

$$k_{cyc,low\,T}(T) = k_{cyc,low\,T,ref} * e^{[\frac{E_{a,cyc,low\,T}}{R}(\frac{1}{T} - \frac{1}{T_{ref}})]} * e^{[\beta_{low\,T} * \frac{I_{ch} - I_{ch,ref}}{C_o}]} \tag{4.29}$$

where,
$E_{a,cyc,low\ T}$ → activation energy for cyclic ageing at low temperature
R → universal gas constant ($= 8.314 \frac{J}{molK}$)
T → temperature (K)
T_{ref} → reference temperature ($= 298.15K$)
$\beta_{low\ T}$ → equation constant
I_{ch} → charging current (A)
$I_{ch,ref}$ → reference charging current
C_o → cell capacity

$$Q_{L,cyc} = Q_{L,cyc,high\ T} + Q_{L,cyc,low\ T} \tag{4.30}$$

$$Q_L = Q_{L,cal} + Q_{L,cyc} \tag{4.31}$$

Stress Factor	Range
Calendar Ageing	
Temperature	$0°C$, $10°C$, $15°C$, $25°C$, $35°C$, $45°C$, $55°C$
SoC	0%, 12.5%, 25%, 37.5%, 50%, 62.5%, 75%, 87.5%, 100%
Time	$\approx 230\ days$
Cyclic Ageing	
C-rate	$0.25C$, $0.5C$, $1C$
Temperature	$0°C$, $10°C$, $15°C$, $25°C$, $35°C$, $45°C$, $55°C$
Number of cycles	$\approx 2800\ FEC$

Table 4.16: Stress factors and their range for model 6 [48]

4.9.1. Verification - Model 6

The model presented in Section 4.9 was used to recreate the experimental tests, to make sure the model matched the results of the experimental data. As can be seen, Table 4.17 shows that the model outputs (which are in terms of percentage capacity lost) are very close to the experimental output.

Experimental Conditions	Experimental Result	Model Output	Linearized Model Output
Calendar Ageing			
$45°C$, 100% SoC	$\approx 7.8\%$	8.0704%	8.0709%
$25°C$, 100% SoC	$\approx 4.5\%$	4.7874%	4.7877%
Cyclic Ageing			
$55°C$, $0.5C$, 200 FEC	$\approx 1.6\%$	1.7184%	1.7316%
$10°C$, $0.25C$, 100 FEC	$\approx 0.6\%$	0.4915%	0.4981%

Table 4.17: Experiment and model outputs compared for model 6

4.10. Model 7

Petit et al. created an empirical battery degradation model based on calendar and cyclic ageing data obtained from different sources [49, 52, 54]. Both models use the Arrhenius equation to represent the temperature effect with the pre-exponential factor in the case of calendar ageing being SoC dependent and in the case of cyclic ageing being current dependent. Equations 4.32 & 4.33 represent the calendar and cyclic ageing components respectively of model 7.

$$Q_{loss}^{cal} = B_{cal}(SoC) * e^{-\frac{Ea_{cal}}{RT}} * t^{z_{cal}} \tag{4.32}$$

where,
Q_{loss}^{cal} → percentage capacity loss due to calendar ageing

$B_{cal}(SoC)$ → pre-exponential factor dependent on SoC ($= 7.34{*}10^5$ @ $30\%\ SoC$, $= 6.75{*}10^5$ @ $65\%\ SoC$, $= 2.18 * 10^5$ @ $100\%\ SoC$)
Ea_{cal} → activation energy for calendar ageing
z_{cal} → time factor for calendar ageing
R → gas constant ($= 8.314\ \frac{J}{molK}$)
T → temperature (K)

$$Q_{loss}^{cyc} = B_{cyc}(I) * e^{\frac{-Ea_{cyc}+\alpha|I|}{RT}} * Ah^{z_{cyc}} \tag{4.33}$$

where,
Q_{loss}^{cyc} → percentage capacity loss due to cyclic ageing
$B_{cyc}(I)$ → pre-exponential factor dependent on current ($= 3.16 * 10^3$ @ $1A$, $= 2.17 * 10^4$ @ $4A$, $= 1.29 * 10^4$ @ $12A$, $= 1.55 * 10^4$ @ $20A$)
Ea_{cyc} → activation energy for cyclic ageing
z_{cyc} → time factor for cyclic ageing
α → coefficient for ageing acceleration ($= 370.3$)
$|I|$ → absolute value of current flowing through the cell during a cycle
R → gas constant ($= 8.314\ \frac{J}{molK}$)
T → temperature (K)

Stress Factor	Range
Calendar Ageing	
Temperature	$30°C, 45°C, 60°C$
SoC	$30\%, 65\%, 100\%$
Time	$\approx 230\ days$
Cyclic Ageing	
C-rate	$0.5C, 2C, 0C, 10C$
DoD	$10\%, 20\%, 50\%, 80\%, 90\%$
Temperature	$-30°C, 0°C, 15°C, 25°C, 45°C, 60°C$
Number of cycles	$\approx 1000\ FEC$

Table 4.18: Stress factors and their range for model 7 [52, 54]

4.10.1. Verification - Model 7

The model described in Section 4.10 was tested by attempting to replicate the results of the experiments conducted in [52] & [54]. It must be noted that the value of $B_{cyc}(I)$ provided in [49] was $3.16 * 10^3$, however, in [54] from which the experimental data points are extracted, the value of $B_{cyc}(I)$ was $3.16 * 10^4$ for a current of $1A$. The value put forward in [54] was thereafter proven to be correct in the experimental verification, therefore the results displayed in Table 4.19 reflect the correct $B_{cyc}(I)$ value of $3.16 * 10^4$. As can be seen in Table 4.19, the model outputs (which are in terms of percentage capacity lost) are very close to the experimental observations, therefore verifying the model.

Experimental Conditions	Experimental Result	Model Output	Linearized Model Output
Calendar Ageing			
$45°C, 30\%\ SoC$	$\approx 12\%$	11.2497%	11.2497%
$30°C, 65\%\ SoC$	$\approx 2.5\%$	2.6223%	2.6223%
Cyclic Ageing			
$60°C, 0.5C, 10\% DoD$	$\approx 15\%$	15.2764%	15.3851%
$60°C, 0.5C, 20\% DoD$	$\approx 22.5\%$	22.3659%	22.4760%

Table 4.19: Experiment and model outputs compared for model 7

4.11. Review of Research Goals

In this chapter, the following aspects of the research goals were addressed:

- Each model was introduced and verified by applying the experimental conditions to the model. The model was deemed accurate if the predicted degradation level by the model matched the experimental observations. In certain cases such as models 2, 3 & 7 where errors were found during the verification process, the models were adjusted such that the experimental observations were matched
- Time and throughput were identified as unique stress factors in the application of irregular power profiles to empirical/semi-empirical models and were subsequently dealt with using linearized forms of the model equations
- Irregular power profiles also caused problems related to the definition of a cycle. The usual method is to use rainflow counting, however a different method was used in this study

5

Analysis

While Chapter 2 introduced the important concepts associated with battery degradation, Chapter 3 introduced the real world power profile being used to compare and analyze the models and Chapter 4 detailed the specific models under study. This chapter aims to analyze and compare these models. To this effect, the models were analyzed to understand how different stress factors affect the output of these models and how different models when used under the same operating conditions lead to different results.

5.1. Assessing Calendar Ageing Models

In this section, the calendar ageing models implemented in MATLAB are assessed in two ways. First, the relationships described between stress factors and calendar ageing in Section 2.2 were used to understand how the experimental tests done in each calendar ageing model affect the accuracy and usability for each model. Second, the yearlong power profile described in Section 3.3 was applied to each model verified or corrected as shown in Chapter 4. Given that the same power profile scaled to the cell in question was used, the differences in output were attempted to be explained.

Model #	Stress Factors	
	Temperature	SoC
1	$35°C$, $40°C$, $50°C$	0%, 10%, 20%, 30%, 50%, 60%, 70%, 80%, 85%, 90%, 95%
2	$10°C$, $22°C$, $34°C$, $46°C$	NA
3	$30°C$, $45°C$, $60°C$	30%, 65%, 100%
5	$40°C$, $47°C$, $55°C$	10%, 50%, 90%
6	$0°C$, $10°C$, $15°C$, $25°C$, $35°C$, $45°C$, $55°C$	0%, 12.5%, 25%, 37.5%, 50%, 62.5%, 75%, 87.5%, 100%
7	$30°C$, $45°C$, $60°C$	30%, 65%, 100%

Table 5.1: Stress factor ranges and percentage capacity losses for calendar ageing models

5.1.1. Model 1

The accelerated calendar ageing tests conducted by the authors of model 1 consider elevated temperatures as shown in Table 5.1. The important points regarding this model are as follows:

- Of the accelerated ageing test data collected, the maximum data was collected for the highest temperature of $50°C$. As Section 2.2.2 clearly indicates, the degradation mechanism occurring at high temperatures (such as at $50°C$) is different from that at lower temperatures (such as at room temperature). Therefore, the data collected shows a heavy bias towards the greater levels of degradation occurring at elevated temperatures and is likely to overestimate the degradation taking place at lower temperatures as a result

- With respect to SoC, the tests run cover the entire SoC range in a high level of detail, therefore the plateau regions indicated in Section 2.2.3 are likely well captured leading to an accurate estimation of the SoC effect on calendar ageing
- The best use case for this calendar ageing model is therefore at elevated temperatures (such as those tested) over the entire SoC range

5.1.2. Model 2

The authors of model 2 consider two stress factors to affect calendar ageing, namely, time and temperature. The important points to note about this model are as follows:

- The SoC of the cell has been omitted as a stress factor
- Temperature dependence, as in the case of model 1 was based on the Arrhenius function. It is of critical importance to note that the test matrix used to build model 2 contained no calendar ageing test data, therefore the authors used low-impact cyclic ageing (low c-rate of $0.5C$ and DoD of 10%) to represent calendar ageing. Therefore, no real storage SoC dependency could be established for this model. The use of cyclic ageing data is also most likely to cause elevated estimations of calendar ageing
- As will be noted later on, the higher than normal reported calendar ageing will also affect the cyclic ageing estimations
- Given the observations made, this calendar ageing model cannot be recommended for use under any conditions

5.1.3. Model 3

Model 3 was created based on Dakin's degradation approach, a significantly different method when compared to models 1 & 2. Equation 4.13 shows the calendar ageing equation adopted where parameter b represented the activation energy as present in the Arrhenius equation. The important points to note regarding this model are as follows:

- As detailed in Section 4.6.1, the calendar ageing equation had to be heavily modified for the experimental observations to be replicated by the model, with Eqn 4.18 representing the new calendar ageing model. Unfortunately, this model bears little to no resemblance to the Arrhenius equation generally used for calendar ageing models
- It is important to note that the experimental data collected for this cell was also accelerated ageing test data (similar to model 1 and many other models) and therefore suffers the same deficiencies relating to the temperature effect on calendar ageing. Table 5.1 also shows that only three SoCs were considered in the ageing tests done, therefore possibly leading to an erroneous depiction of the SoC effect as described in Section 2.2.3
- The observations made make it clear that the best usage case for this calendar ageing model would be at elevated temperatures to estimate ageing only at the SoCs tested

5.1.4. Model 5

Just like in the case of model 1, the authors of model 5 performed accelerated ageing tests to obtain the necessary experimental data required for their model. The important points regarding this model are as follows:

- Table 5.1 shows that the temperatures used during experimentation reached and crossed the threshold temperature for SEI breakdown. It must be noted that there is a bias towards $55°C$ with the maximum number of data points being obtained at this temperature
- On the SoC data, again there is a paucity in the number of different SoCs tested leading to an incorrect representation of the degree of lithiation of the anode and hence an incorrect estimation of calendar ageing
- Given the observations made, just as in the case of model 3, the best use case of model 5 remains at high temperatures and SoCs tested as shown in Table 5.1

5.1.5. Model 6

The authors of model 6 have taken a wide range of SoCs and temperatures in the calendar ageing tests as shown in Table 5.1. The important points regarding this model are as follows:

- The range of temperatures tested covers two different mechanisms, one at lower temperatures that involves the formation of the SEI and one at higher temperatures that involves the breakdown and creation of a second SEI. It is unlikely that the mechanism at higher temperatures is represented by the Arrhenius equation (which is used in this model), therefore the most accurate representation of the temperature effect would involve separate equations for the two different mechanisms involved (as was followed in the cyclic ageing section of the very same model, detailed in Section 4.9
- With respect to the SoC effect, the calendar ageing model takes into account the degree of lithiation of the electrode along with a wide spread of SoC data, therefore it is most likely to have an accurate representation of the calendar ageing caused due to SoC of the cell
- The best use case for this model would therefore be at regular temperatures (below the breakdown of the SEI) over the entire SoC range

5.1.6. Model 7

Model 7 uses calendar ageing data from the SIMCAL project, the data for which is shown in [52]. As can be seen in Table 5.1, three temperatures and three SoCs were tested. The points to note regarding this model are as follows:

- Due to the temperatures being covered, both the lower temperature and higher temperature mechanisms will be present in the experimental data. Although the model uses the Arrhenius equation to describe the temperature dependence, a different method is probably required to determine the temperature effect on calendar ageing at high temperatures
- As far as SoC is concerned, the model uses different values of the pre-exponential factor and activation energy (in the Arrhenius equation) for the three different temperatures. However, the lack of SoCs tested does not allow the model to provide an accurate depiction of the SoC effect
- Due to the nature of the experimental data, the best use case for this model would be at temperatures of between $30 - 40°C$ at the specific SoCs tested

5.1.7. Comparison of Calendar Ageing Results

Model #	Capacity Loss (%)
1	1.0650%
2	8.9066%
3	0.9651%
5	2.5954%
6	3.5884%
7	0.5612%

Table 5.2: Percentage capacity loss due to calendar ageing for all models

Table 5.2 shows the percentage capacity loss due to calendar ageing estimated by each model at a temperature of $11°C$ (average yearly temperature in the Netherlands) and a maximum cell SoC of 80% with Fig 5.1 showing the drop in capacity over time. Although every model is subjected to the same operating conditions and power profile scaled based on the cell being used, there is a marked difference in their output. The main points to note regarding this are as follows:

- Model 2 is the outlier with a much higher estimated degradation than any other model. This is attributed to the fact that the data points used to build the model are mild cyclic ageing data points as highlighted in Section 5.1.2.

- Model 3 was extensively revised during the validation process as detailed in Section 4.6.1. Neither the revised model 3 nor the model 5 calendar ageing equations bear any resemblance to the Arrhenius equation and are therefore entirely empirical in nature. Therefore, it is difficult to explain exactly why their predicted capacity loss values are so different.
- Models 1, 6 & 7 all use Arrhenius type equations to define the temperature effect on calendar ageing. While model 6 uses the Tafel equation to describe the SoC effect, models 1 and 7 both use the pre-exponential factor to define the SoC effect. The difference between the two models is that while model 1 constantly changes the value of the pre-exponential factor with SoC (cell voltage), model 7 has fixed values of the pre-exponential factor for SoCs of 30%, 65% & 100% SoCs. It must also be noted that between the three models, model 7 which has the highest (average) activation energy has the lowest estimated degradation, while model 6 which has the lowest value of activation energy (almost one-third that of model 1) has significantly higher estimated degradation.

5.2. Assessing Cyclic Ageing Models

In this section, the cyclic ageing models implemented in MATLAB are assessed in two ways. First, the relationships described between stress factors and calendar ageing in Section 2.3 were used to understand how the experimental tests done in each calendar ageing model affect the accuracy and usability for each model. Second, the yearlong power profile described in Section 3.3 was applied to each model verified or corrected as shown in Chapter 4. Given that the same power profile scaled to the cell in question was used, the differences in output were attempted to be explained.

Model #	Stress Factors			
	Temperature	**C-Rate**	**Mean SoC**	**DoD**
1	$35°C$	$1C$	10%, 25%, 50%, 65%, 75%, 80%, 90%, 95%	5%, 10%, 20%, 50%, 80%, 100%
2	$10°C$, $22°C$, $34°C$, $46°C$	$0.5C$, $1C$, $2C$, $3.5C$, $5C$, $6.5C$	NA	50%
4	$25°C$, $35°C$, $45°C$	$1C$	50%	100%
5	$35°C$, $42°C$, $50°C$	$4C$	50%	10%, 45%, 80%
6	$0°C$, $10°C$, $15°C$, $25°C$, $35°C$, $45°C$, $55°C$	$0.25C$, $0.5C$, $1C$	50%	100%
7	$-30°C$, $0°C$, $15°C$, $25°C$, $45°C$, $60°C$	$0.5C$, $2C$, $6C$, $10C$	NA	10%, 20%, 50%, 80%, 90%

Table 5.3: Stress factor ranges and percentage capacity losses for cyclic ageing models

5.2.1. Calendar Ageing Effect

An important point to note is that all cyclic ageing data collected during the experimentation phase contains a calendar ageing component as well. This data therefore is not 'pure' cyclic ageing data. The standard practice is as follows:

- Calendar and cyclic ageing tests are performed to obtained data points based on which empirical/semi-empirical models are built
- The calendar ageing data is used to build the calendar ageing model
- 'Pure' cyclic ageing data is obtained by using the calendar ageing model to remove the calendar ageing portion from the experimental cyclic ageing data
- The 'pure' cyclic ageing data is then used to build the cyclic ageing model

Although this is the procedure followed in most models [27, 44], it is not always the case. This could possibly lead to erroneous estimations of cyclic and by extension total ageing as well.

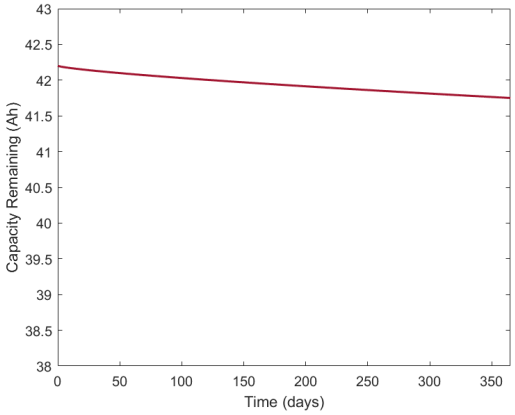

(a) Calendar ageing over a 1 year period for model 1

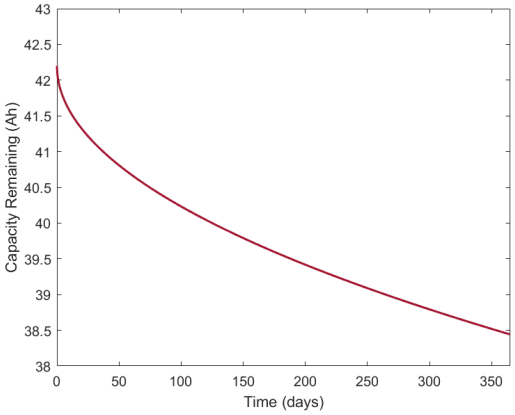

(b) Calendar ageing over a 1 year period for model 2

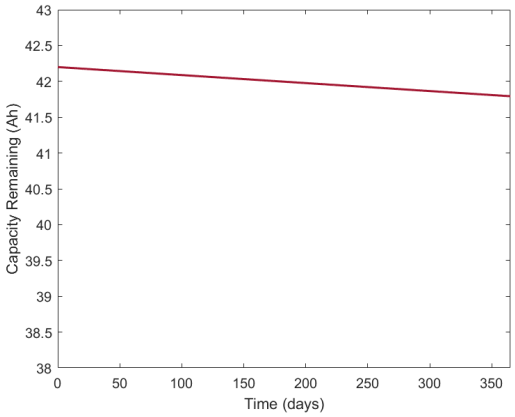

(c) Calendar ageing over a 1 year period for model 3

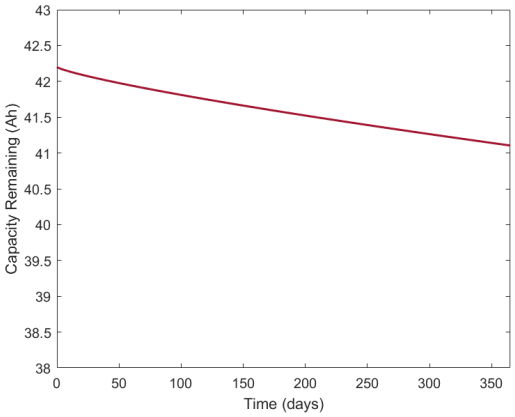

(d) Calendar ageing over a 1 year period for model 5

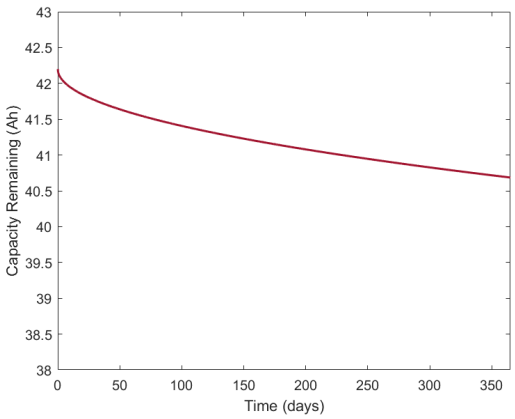

(e) Calendar ageing over a 1 year period for model 6

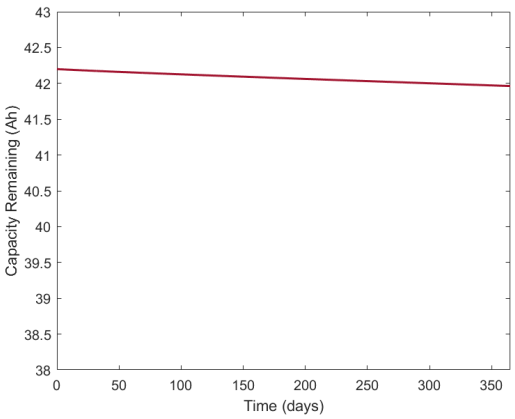

(f) Calendar ageing over a 1 year period for model 7

Figure 5.1: Calendar ageing for each model when the yearlong power profile (Section 3.3) is applied

5.2.2. Model 1

Schmalstieg et al. [27] focused their cyclic ageing experimental conditions on two factors, mean SoC and DoD. As is shown in Table 5.3, a large range of mean SoC and DoD are considered, all at a fixed temperature of $35°C$ and a C-rate of 1C. The highlights of this model are as follows:

- The conditions of the yearlong profile include low c-rates, low DoDs and a high mean SoC. Given the experimental data generally covers this criteria, this model is likely to be quite accurate for the specific power profile created
- In applications where the working conditions are below room temperature and/or with high C-rates, the model is likely to be much less accurate. As detailed in Sections 2.3.2 & 2.3.3, the degradation mechanisms that take place under these conditions are different (and not covered by the test data) therefore likely causing a loss in accuracy

5.2.3. Model 2

Table 5.3 shows that the authors of model 2 paid particular attention to temperature and c-rate. Although data was collected for several different DoDs, only the data for 50% DoD was used in the fitting for the model. Along with this it must be noted that the mean SoC around which these cycles took place was unavailable. The important points regarding this model are:

- Since neither the mean nor start SoC of the cyclic ageing tests conducted is available, it is possible that the data collected during experimentation was in regions of relatively low electrode volume change as discussed in Section 2.3.4, therefore making the model less accurate in other regions.
- Section 5.1.2 details that the experimental data used for the calendar ageing model was in reality low impact cyclic ageing data that therefore led to an overestimation of calendar ageing by the model. Based on Section 5.2.1 any overestimation by the calendar ageing model would likely corrupt the 'pure' cyclic ageing data points, leading to an underestimation by the cyclic ageing model.

It is also possible that a combination of the two reasons above is responsible for the extremely low cyclic ageing estimation. The best use case for this model would be in scenarios where the operating temperature and c-rate fluctuate significantly given that the experimental data covers the multiple mechanisms both these stress factors involve.

5.2.4. Model 4

The focus of model 4, as made clear in Table 5.3 is the effect of temperature. Since the entire temperature range tested lies at or above room temperature, the Arrhenius equation which was used to model the temperature effect is valid. The rest of the stress factors are not very well represented however, with only one c-rate, one mean SoC and one DoD being tested. The important points regarding this model are as follows:

- Since all cyclic ageing tests were conducted for 100% DoD it is possible that both effects described in 2.3.4 have been picked up in the experimental data. The real world power profile subjects the cell to much smaller DoDs and high mean SoCs, therefore possibly only one of the effects described is encountered. This would therefore lead to an overestimation of the cyclic ageing by the model.
- Section 5.2.1 explains how 'pure' cyclic ageing data is obtained prior to building a cyclic ageing model. Since [46] does not conduct any calendar ageing tests, it was not possible for them to remove the calendar ageing effect. Therefore, the model built is also likely to overestimate cyclic ageing in all cases (as it also includes the calendar ageing effect).

Both points above indicate that the best application for model 4 is for use cases where temperature is varied (above room temperature) with low c-rates and 100% DoD. Even in these conditions it must be noted that the effect of calendar ageing is still present and the model is likely to overestimate cyclic ageing as a result.

5.2.5. Model 5

Model 5 is a purely empirical model with three important points to note:

- All the cyclic ageing tests are done at a c-rate of $4C$ after which c-rate is not considered in the cyclic ageing model (temperature, cycle depth and number of cycles are the only considered factors). A data set of consisting purely of high c-rate test data is likely to yield a model that will overestimate the capacity fade at lower c-rates.
- The model uses number of cycles as a stress factor as opposed to cell throughput. As detailed in Section 4.2, the method used to define cycles in this study in unique to the demands of an irregular power profile, while the input number of cycles required in the model potentially uses an alternative method (not detailed in [47]).
- Section 5.2.1 highlights the problem with models that do not separate out the 'pure' cyclic ageing data in the experimental phase. Model 5 faces the same issue, as a result of which calendar ageing is included in the cyclic ageing estimation.

As a result of the points mentioned above, the only use case that can be seen for this model is scenarios where fast charging and discharging is occurring in a regular manner (therefore the number of cycles is clear).

5.2.6. Model 6

The cyclic ageing modelling done for model 6 considers three different conditions:

- High temperatures where the effects of temperature dominate over that of c-rate
- Low temperatures where the effects of c-rate dominate over those of temperature
- High mean SoC where the transition from stage 2 to stage 1 plays an important role

[48] states that the mechanisms occurring in each case are different, necessitating each to be modelled separately. This is a unique approach, and the salient points regarding this model are as follows:

- In the high SoC case, the reference mean SoC is taken as 82%, meaning the mechanism that causes accelerated degradation at high SoCs only occurs at mean SoCs above 82%. Given that the maximum charge that the cell reaches in the simulation of the yearlong power profile is 80% and that [36] show the highest degradation to occur at a mean SoC of 75%, it is likely that model 5 does not accurately portray the accelerated ageing caused by the stage 2 to stage 1 transition occurring when the yearlong power profile is used, even though it aims to do so
- It must be noted that the high degradation encountered during low SoC, shallow DoD cycling conditions as explained in Section 2.3.4 is not taken into account in this model
- The best use cases for this model are in conditions of variable temperature and c-rate but mean SoCs and DoDs that do not touch the accelerated ageing mechanisms that occur at low SoC, shallow DoD conditions or SoCs where the stage 2 to stage 1 transition occurs at the anode

5.2.7. Model 7

The authors of model 7 used data (and to some extent the model) present in [54]. Table 5.3 shows the range of test conditions considered in the experimental data of [54]. As can be seen, a very wide range of conditions are covered, and although the mean SoC for the cyclic ageing tests is unavailable, the range of DoDs show that almost the entire range of SoC is considered. There are a few important points to note regarding this model:

- The calendar ageing effect on cyclic data points (as described in Section 5.2.1) is not considered which would potentially lead to an overestimation of the actual cyclic ageing.
- Wang et al. [54] from where the data points have been sourced note that at low c-rates ($0.5C$), the effect of DoD is not very strong. As stated previously however, [36] & [35] show otherwise. It is possible that the cyclic ageing tests conducted do not discharge the cell at any point, therefore missing the degradation mechanism highlighted in [35], but no hypotheses can be provided as to the points noted in [36].

Although the range of test data would lead to the conclusion of a robust model with wide ranging use cases, the two points noted above lead to certain doubts. It is therefore inconclusive how accurate and useful model 7 is.

5.2.8. Comparison of Cyclic Ageing Results

Model #	Capacity Loss (%)
1	3.1599%
2	0.6279%
4	6.5290%
5	19.0976%
6	0.7944%
7	1.7917%

Table 5.4: Percentage capacity loss due to cyclic ageing for all models

Table 5.4 shows the percentage degradation due to cyclic ageing estimated by each model with Fig 5.2 showing the drop in capacity from the inital capacity over time. The operating conditions were the same as described in Section 5.1.7. As was the case with the calendar ageing comparison, the results for all the models were different despite the same conditions being applied in each case. Given that cyclic ageing is generally a more complex phenomenon with multiple stress factors interdependent on each other, as well as different stress factors considered in each model; comparing the results is an altogether more complicated task. The salient points regarding this are as follows:

- The outlier in the case of the cyclic ageing results was model 5. The abnormally high predicted degradation can be attributed to the test data used to build the model. All the cyclic ageing experiments conducted for this model were performed at a c-rate $4C$, potentially leading to over-estimation of degradation at lower c-rates.

- Among the remaining models, throughput was the only common stress factor considered in every equation. All models use a power law relationship to define the throughput with the power varying from $0.5 - 1.317$. Unfortunately, no clear trend with respect to throughput is noticed.

- Both models 4 & 7 use Arrhenius type equations to define the temperature effect on cyclic ageing and as such can be compared. Model 7, however, also includes absolute value of current as an additional stress factor within the Arrhenius type equation. A significant point to note is that the value of the pre-exponential factor in the case of model 4 is two orders of magnitude higher than that of model 7 (at low c-rates). This is likely to have played a significant role in the estimated degradation of model 4 being much higher than that of model 7. Another factor to have played a role is the power in the power law relationship defining the throughput effect. The power of throughput is 1.317 in model 4 versus 0.55 in model 7. It must however be highlighted at this point that the Arrhenius equation is generally agreed to be a good representation of the temperature effect at room temperature (generally $25°C$) and above. The temperature these models were tested at was lower than this.

- Important to note is that the only model to consider mean SoC and DoD as stress factors in the degradation equation is model 1. Although other models do consider different mean SoCs and DoDs in their experimental data prior to building the model, the stress factors are not present in the final degradation equation itself. Ignoring models 4 & 5 (whose high predicted degradation levels are explained above), model 1 has the highest level of degradation. It is possible that the inclusion of these stress factors is playing a role in the degradation estimation.

- The only models to include c-rate as a stress factor in some form were models 2, 6 & 7. As can be seen in Table 5.4, these three models also estimate the minimum amount of degradation. This may also be a factor in the degradation estimation.

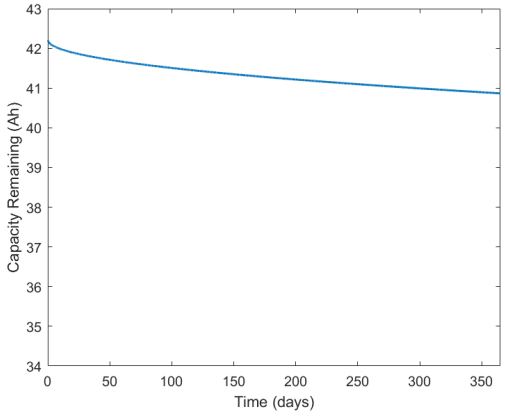

(a) Cyclic ageing over a 1 year period for model 1

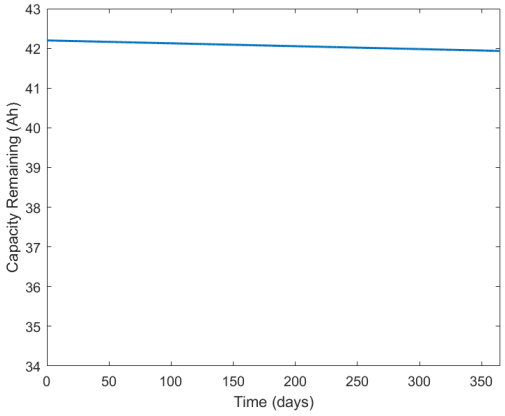

(b) Cyclic ageing over a 1 year period for model 2

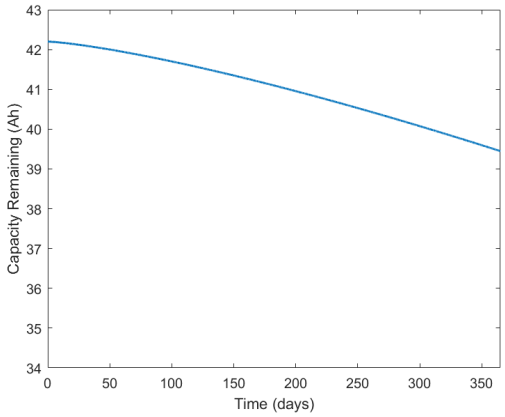

(c) Cyclic ageing over a 1 year period for model 4

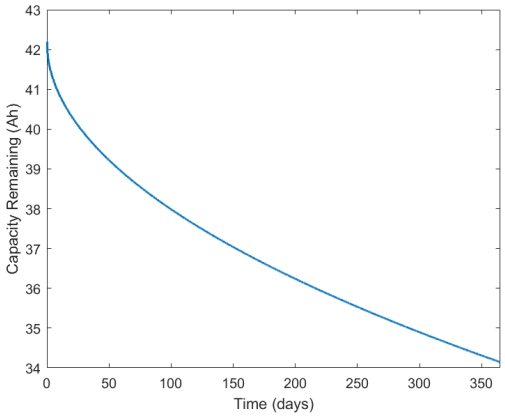

(d) Cyclic ageing over a 1 year period for model 5

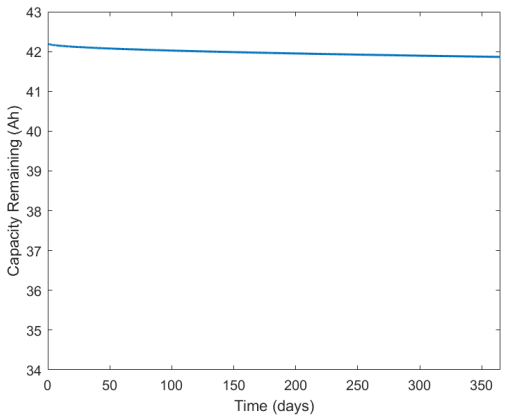

(e) Cyclic ageing over a 1 year period for model 6

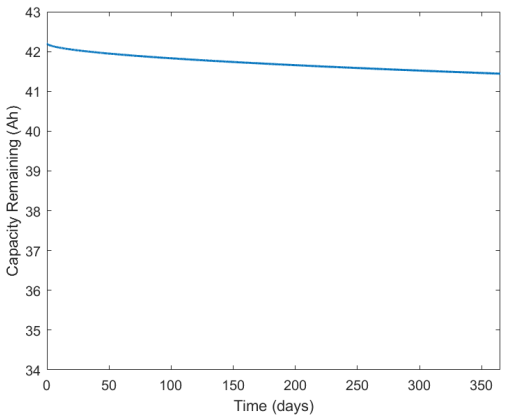

(f) Cyclic ageing over a 1 year period for model 7

Figure 5.2: Cyclic ageing for each model when the yearlong power profile (Section 3.3) is applied

5.3. Summary and Toolbox

5.3.1. Summary

Table 5.5 summarizes the best use case for each calendar and cyclic ageing model separately, as previously discussed in Sections 5.1 & 5.2. A few points to note regarding the best use case summary are:

- With respect to calendar ageing, there are models that perform accelerated ageing tests (where the degradation mechanism is different from that at lower temperatures) therefore leaving them only usable at these temperatures. However, these models may still use the Arrhenius equation to depict the temperature effect, which is not entirely accurate given the Arrhenius equation does not accurately represent the alternate degradation method taking place. Hence, the use of these models at high temperatures could be affected by this factor.
- With respect to cyclic ageing, there are certain models that do not remove the calendar ageing portion that occurs during cyclic ageing. Therefore, although these models may be applicable in certain scenarios based on the testing conditions, the caveat is that the predicted degradation might still be an overestimation due to the calendar ageing effect.

Model #	Calendar Ageing	Cyclic Ageing
1	Accelerated ageing tests conducted by the authors render this calendar ageing model useful only at elevated temperatures ($\approx 50°C$), but over the entire SoC range	Model 1 covers a wide range of SoCs and DoDs, but only one temperature and c-rate. Therefore, the best use case for this model is at temperatures above room temperature, low c-rates but over the entire SoC range
2	This calendar ageing model is hurt by the fact that the data used for this model is low impact cyclic ageing data. The use of this data leads to the model overestimating calendar ageing, leaving it unsuitable for use in any circumstances	The overestimation of calendar ageing results could lead to an underestimation of the cyclic ageing results as mentioned in Section 5.2.3. Therefore, the usefulness of the cyclic ageing is questionable
3	Although the model was heavily modified in the verification section (Section 4.6.1). Unfortunately, the use of accelerated testing conditions leads to this model only being useful at high temperatures, at the few SoCs tested	NA
4	NA	Given that all the tests conducted were at 100% DoD the best use case for this model is in conditions above room temperature where the use case involves fully charging and discharging the cell. The model also does not separate the calendar ageing effect, which means that even in those conditions, the degradation estimation is likely to be higher than in reality

5	Model 5 is similar to model 3 in that accelerated conditions are tested at only 3 SoCs. Therefore, the use case of model 5 remains at high temperatures and SoCs tested by the authors	Model 5 uses extremely high c-rates in testing, as well as requiring the number of cycles as a stress factor. Therefore, the only use case for this model is fast charge-discharge scenarios with regular cycles
6	Model 6 takes into account the most comprehensive range of testing data. As a result, the model can be used at regular temperatures and the full range of SoC	Model 6 represents the effects of temperature and c-rate well, but the effects of SoC and DoD are not very well expressed. Therefore, this model can be used over a wide range of temperatures and c-rates, but only cycled where accelerated ageing mechanisms do not come into play
7	Given that model 7 uses the Arrhenius equation to model the temperature effect and the majority of testing points are below the SEI breakdown threshold, the best use case for this model is above room temperature and below $\approx 50°C$, only at the SoCs tested	The use case for this model is an unknown due to the points mentioned in Section 5.2.7

Table 5.5: Summary of best use cases for each model

5.3.2. Toolbox

Having verified and implemented seven different models using a unique implementation method along with analyzing each model to understand its best use scenario, the goal of the toolbox was to bring these aspects together such that any user may both use the toolbox to implement any model of their choice as well as understand where the model chosen is most effective. The main points of the toolbox are as follows:

- The toolbox begins with a short description of the source of each model
- Next, the power profile derived from the WLTP cycle as detailed in Section 3.3 in explained in brief
- Users are given the option of entering the temperature at which they would like to run the model, the highest SoC to which the cell should be charged and the model to be tested
- Once the operating conditions and model are chosen by the user, the toolbox provides the estimated calendar, cyclic and total ageing as a percentage. Total ageing is simply calculated as the summation of calendar and cyclic ageing. Along with this, the toolbox also provides a graph of the drop in capacity over time as shown in Fig 5.3.
- Finally the toolbox displays the best use case for the model in question, similar to Table 5.5

5.4. Review of Research Goals

In this chapter, the following aspects of the research goals were addressed:

- Each model was analyzed to understand how stress factors and degradation phenomena affect the use case for each model

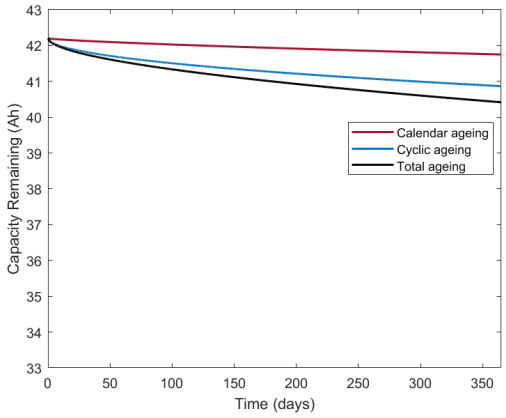

(a) Calendar, cyclic and total ageing over a 1 year period for model 1

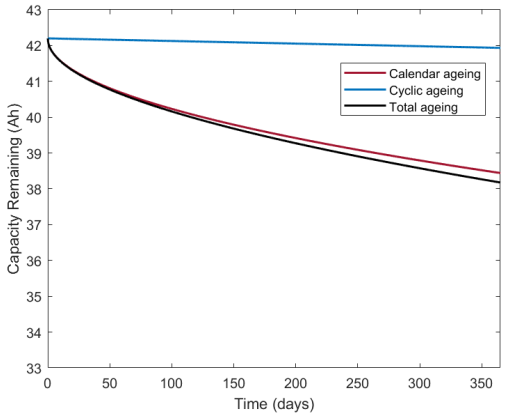

(b) Calendar, cyclic and total ageing over a 1 year period for model 2

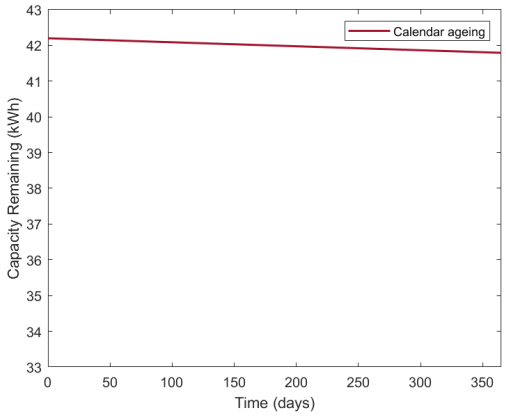

(c) Calendar, cyclic and total ageing over a 1 year period for model 3

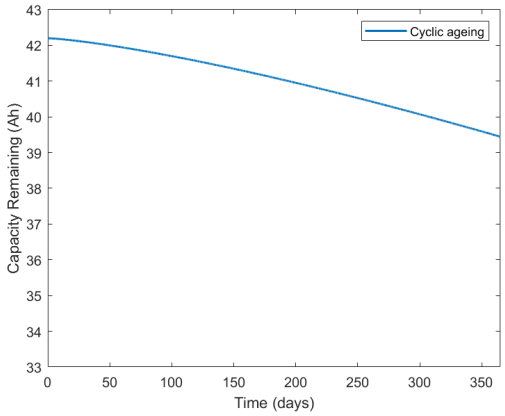

(d) Calendar, cyclic and total ageing over a 1 year period for model 4

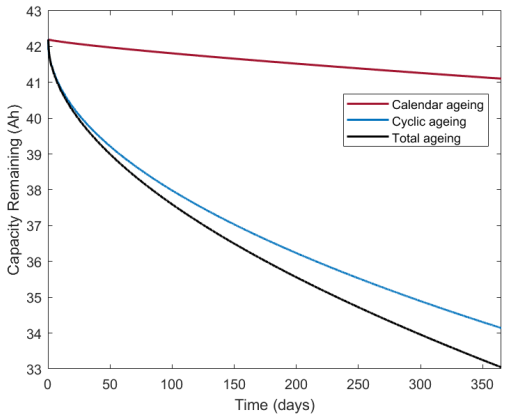

(e) Calendar, cyclic and total ageing over a 1 year period for model 5

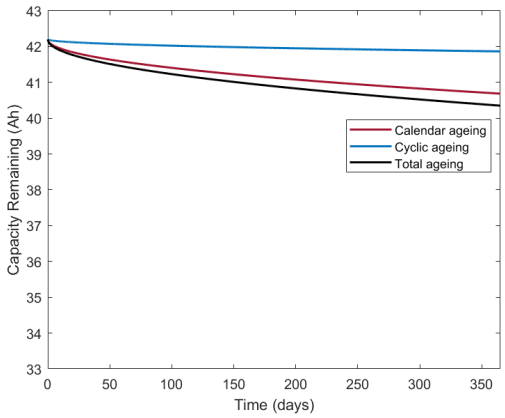

(f) Calendar, cyclic and total ageing over a 1 year period for model 6

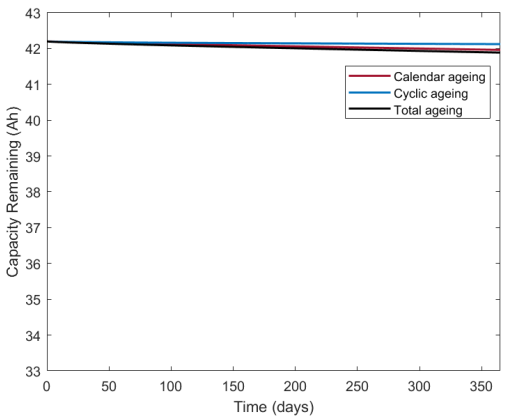

(g) Calendar, cyclic and total ageing over a 1 year period for model 7

Figure 5.3: Calendar, cyclic and total ageing for each model when the yearlong power profile (Section 3.3) is applied

- The common power profile built was applied to each model after the batteries were equalized. The difference in output for identical testing conditions was explained
- A toolbox was built in MATLAB to allow users to understand the outputs and best use scenarios for the models studied

6

Conclusion

The goal of this study was to investigate different empirical/semi-empirical models that exist in literature, understand how they could be applied in a real-world scenario, compare their outputs in an identical use case and build a toolbox that could better explain to a user how these models may be applied. Here, the research questions first introduced in Chapter 1 are gone through in detail:

- ***What are the stress factors that effect battery degradation and what effect do they have?***

  Chapter 2 introduced the concepts of calendar (degradation occurring when no current flows through the cell) and cyclic (degradation occurring when the cell is in use) ageing, each of which have their own stress factors. Calendar ageing is dependent on time, temperature and SoC while cyclic ageing is dependent on throughput, temperature, c-rate, mean SoC and DoD. The relationships between these stress factors and degradation is governed by the effect these stress factors have on degradation phenomena such as the formation of the SEI or volume changes in the anode. It is also important to note that stress factors, especially in the case of cyclic ageing are interdependent with each other. This chapter also introduced the different kinds of degradation models in literature, with the focus being on empirical/semi-empirical models for the rest of the study.

- ***How are empirical models applied in real world conditions?***

  Empirical/semi-empirical models are built on experimental data created from tests under static conditions. For calendar ageing, this means a cell is stored at a particular temperature and SoC, and degradation after a certain amount of time is recorded. For cyclic ageing, a cell is cycled at a particular c-rate, temperature and DoD and degradation after a certain amount of time is recorded. In real-world conditions the use cases are much more dynamic. This therefore led to the creation of an implementation method designed for irregular power profiles. In Chapter 4, time and throughput were identified as unique stress factors due to their constantly increasing nature as well as their dependence on prior data. The models were therefore linearized with respect to time for calendar ageing and throughput for cyclic ageing to account for these two stress factors in an irregular power profile. The second challenge thrown up by irregular power profiles was the definition of a ”cycle” for cyclic ageing calculations. Although the usual technique followed in such cases is rainflow counting, this study proposes an alternative method to define a cycle, better suited for use in battery related studies. Chapter 4 also looks into how every model studied was first verified by attempting to replicate experimental degradation results through the model. Errors and inaccuracies were found in models 2, 3 & 7 by this simple technique and were subsequently rectified.

- ***How do the testing conditions affect the use case and outputs of different models?***

  Once Chapters 2, 3 & 4 introduced the principles of battery degradation, the power profile being used and its implementation method & the models under consideration, Chapter 5 brought it all together. Calendar and cyclic ageing degradation were treated separately and it was noted that in both cases, the predicted degradation from the models varied significantly. Sections 5.1.7 &

5.2.8 for calendar and cyclic ageing respectively detail the significant points regarding the comparison, where in some cases the cause of the difference is quite clear, in others it is not as straightforward. Cyclic ageing was found to be more complicated given the interdependencies between different stress factors. Chapter 5 also analyzed each model individually, applying the relationship between stress factors and degradation phenomena detailed in Chapter 2 to better understand how accurate each model was and more importantly, which use cases would be best for each model.

- ***Can a user-friendly method to summarize and understand the use cases of models be built and what would its functionality look like?***

  Section 5.3 of Chapter 5 details a toolbox built in MATLAB. The toolbox combines two different aspects of this study, implementation of an irregular power profile using the method described in Section 4.4 with the analysis of each model. The goal of the toolbox was to enable a user to apply the given power profile to a model of their choice under user defined operating conditions as well as provide information regarding the best use case for that particular model.

6.1. Future Scope

This study has taken a very close look at implementing, analyzing and comparing various empirical/semi-empirical models. However, there are still areas that can be further investigated and improved upon:

- The cycle counting method used in this study attempts to strike a balance between having cycles with a discernible DoD and accurate c-rate along with making physical sense in the context of cell charging/discharging. Further methods taking all these factors into account could also be established.
- The power profile built based on the WLTP drive cycle considers the same distance is driven every day of the year. This could be altered to reflect weekday versus weekend driving habits.
- The MATLAB code for each model considers a constant temperature and does not take into account battery self heating. Both these points could be improved upon.
- All the analysis done and conclusions drawn have no experimental backing, therefore only *potential* reasons could be put forward for model differences and best use scenarios. Although the reasoning is robust, experimental tests could potentially back up the reasoning used.
- The potential relationship between activation energy and estimated calendar ageing noted in Section 5.1.7 requires further study.
- The toolbox can be improved by adding further real-world power profiles, or allowing a user to input their own power profile to be analyzed by a model. Furthermore, even in the toolbox, the temperature once selected by the user is static throughout the duration of the test, this could be altered to include daily and/or seasonal variations.

Bibliography

[1] Atika Qazi et al. “Towards Sustainable Energy: A Systematic Review of Renewable Energy Sources, Technologies, and Public Opinions”. In: *IEEE Access* 7 (2019). Conference Name: IEEE Access, pp. 63837–63851. ISSN: 2169-3536. DOI: 10.1109/ACCESS.2019.2906402.

[2] Lata Tripathi et al. “Renewable energy: An overview on its contribution in current energy scenario of India”. In: *Renewable and Sustainable Energy Reviews* 60 (July 2016), pp. 226–233. ISSN: 13640321. DOI: 10.1016/j.rser.2016.01.047.

[3] Matthew D. Leonard, Efstathios E. Michaelides, and Dimitrios N. Michaelides. “Energy storage needs for the substitution of fossil fuel power plants with renewables”. In: *Renewable Energy* 145 (Jan. 2020), pp. 951–962. ISSN: 09601481. DOI: 10.1016/j.renene.2019.06.066.

[4] E.M.G. Rodrigues et al. “Energy storage systems supporting increased penetration of renewables in islanded systems”. In: *Energy* 75 (Oct. 2014), pp. 265–280. ISSN: 03605442. DOI: 10.1016/j.energy.2014.07.072.

[5] Mohammad Taufiqul Arif, Amanullah M. T. Oo, and A. B. M. Shawkat Ali. “Energy Storage: Applications and Advantages”. In: *Smart Grids: Opportunities, Developments, and Trends*. Ed. by A B M Shawkat Ali. Green Energy and Technology. London: Springer, 2013, pp. 77–108. ISBN: 978-1-4471-5210-1. DOI: 10.1007/978-1-4471-5210-1_4.

[6] K.C. Divya and Jacob Østergaard. “Battery energy storage technology for power systems—An overview”. In: *Electric Power Systems Research* 79.4 (Apr. 2009), pp. 511–520. ISSN: 03787796. DOI: 10.1016/j.epsr.2008.09.017.

[7] Taehoon Kim et al. “Lithium-ion batteries: outlook on present, future, and hybridized technologies”. In: *Journal of Materials Chemistry A* 7.7 (2019). Publisher: Royal Society of Chemistry, pp. 2942–2964. DOI: 10.1039/C8TA10513H.

[8] Masataka Wakihara. “Recent developments in lithium ion batteries”. In: *Materials Science and Engineering: R: Reports* 33.4 (June 1, 2001), pp. 109–134. ISSN: 0927-796X. DOI: 10.1016/S0927-796X(01)00030-4.

[9] Reiner Korthauer, ed. *Lithium-Ion Batteries: Basics and Applications*. Berlin, Heidelberg: Springer Berlin Heidelberg, 2018. ISBN: 978-3-662-53069-6 978-3-662-53071-9. DOI: 10.1007/978-3-662-53071-9.

[10] Wiljan Vermeer, Gautham Ram Chandra Mouli, and Pavol Bauer. “A Comprehensive Review on the Characteristics and Modeling of Lithium-Ion Battery Aging”. In: *IEEE Transactions on Transportation Electrification* 8.2 (June 2022). Conference Name: IEEE Transactions on Transportation Electrification, pp. 2205–2232. ISSN: 2332-7782. DOI: 10.1109/TTE.2021.3138357.

[11] Xuebing Han et al. “A review on the key issues of the lithium ion battery degradation among the whole life cycle”. In: *eTransportation* 1 (Aug. 2019), p. 100005. ISSN: 25901168. DOI: 10.1016/j.etran.2019.100005.

[12] Christoph R. Birkl et al. “Degradation diagnostics for lithium ion cells”. In: *Journal of Power Sources* 341 (Feb. 2017), pp. 373–386. ISSN: 03787753. DOI: 10.1016/j.jpowsour.2016.12.011.

[13] Xuebing Han et al. “A comparative study of commercial lithium ion battery cycle life in electrical vehicle: Aging mechanism identification”. In: *Journal of Power Sources* 251 (Apr. 2014), pp. 38–54. ISSN: 03787753. DOI: 10.1016/j.jpowsour.2013.11.029.

[14] Pankaj Arora, Ralph E. White, and Marc Doyle. “Capacity Fade Mechanisms and Side Reactions in Lithium□Ion Batteries”. In: *Journal of The Electrochemical Society* 145.10 (Oct. 1, 1998). Publisher: IOP Publishing, p. 3647. ISSN: 1945-7111. DOI: 10.1149/1.1838857.

[15] J. Vetter et al. “Ageing mechanisms in lithium-ion batteries”. In: *Journal of Power Sources* 147.1 (Sept. 2005), pp. 269–281. ISSN: 03787753. DOI: 10.1016/j.jpowsour.2005.01.006.

[16] Thomas Waldmann et al. “Temperature dependent ageing mechanisms in Lithium-ion batteries – A Post-Mortem study”. In: *Journal of Power Sources* 262 (Sept. 2014), pp. 129–135. ISSN: 03787753. DOI: 10.1016/j.jpowsour.2014.03.112.

[17] Weishan Li. “Review—An Unpredictable Hazard in Lithium-ion Batteries from Transition Metal Ions: Dissolution from Cathodes, Deposition on Anodes and Elimination Strategies”. In: *Journal of The Electrochemical Society* 167.9 (Jan. 2020). Publisher: The Electrochemical Society, p. 090514. ISSN: 1945-7111. DOI: 10.1149/1945-7111/ab847f.

[18] K. Edström, T. Gustafsson, and J.O. Thomas. “The cathode–electrolyte interface in the Li-ion battery”. In: *Electrochimica Acta* 50.2 (Nov. 2004), pp. 397–403. ISSN: 00134686. DOI: 10.1016/j.electacta.2004.03.049.

[19] Sébastien Grolleau et al. “Calendar aging of commercial graphite/LiFePO4 cell – Predicting capacity fade under time dependent storage conditions”. In: *Journal of Power Sources* 255 (June 2014), pp. 450–458. ISSN: 03787753. DOI: 10.1016/j.jpowsour.2013.11.098.

[20] Julius Schmitt et al. “Impedance change and capacity fade of lithium nickel manganese cobalt oxide-based batteries during calendar aging”. In: *Journal of Power Sources* 353 (June 2017), pp. 183–194. ISSN: 03787753. DOI: 10.1016/j.jpowsour.2017.03.090.

[21] Anna M. Andersson, Kristina Edström, and John O. Thomas. “Characterisation of the ambient and elevated temperature performance of a graphite electrode”. In: *Journal of Power Sources* 81-82 (Sept. 1, 1999), pp. 8–12. ISSN: 0378-7753. DOI: 10.1016/S0378-7753(99)00185-8.

[22] Tao Zheng, Antoni S. Gozdz, and Glenn G. Amatucci. “Reactivity of the Solid Electrolyte Interface on Carbon Electrodes at Elevated Temperatures”. In: *Journal of The Electrochemical Society* 146.11 (Nov. 1, 1999), pp. 4014–4018. ISSN: 0013-4651, 1945-7111. DOI: 10.1149/1.1392585.

[23] M N Richard and J R Dahn. “Accelerating Rate Calorimetry Study on the Thermal Stability of Lithium Intercalated Graphite in Electrolyte”. In: *Journal of The Electrochemical Society* (1999), p. 11.

[24] Peter Keil et al. “Calendar Aging of Lithium-Ion Batteries”. In: *Journal of The Electrochemical Society* 163.9 (July 6, 2016). Publisher: IOP Publishing, A1872. ISSN: 1945-7111. DOI: 10.1149/2.0411609jes.

[25] M. Broussely et al. “Main aging mechanisms in Li ion batteries”. In: *Journal of Power Sources* 146.1 (Aug. 2005), pp. 90–96. ISSN: 03787753. DOI: 10.1016/j.jpowsour.2005.03.172.

[26] Matthieu Dubarry, Nan Qin, and Paul Brooker. “Calendar aging of commercial Li-ion cells of different chemistries – A review”. In: *Current Opinion in Electrochemistry* 9 (June 2018), pp. 106–113. ISSN: 24519103. DOI: 10.1016/j.coelec.2018.05.023.

[27] Johannes Schmalstieg et al. “A holistic aging model for Li(NiMnCo)O2 based 18650 lithium-ion batteries”. In: *Journal of Power Sources* 257 (July 2014), pp. 325–334. ISSN: 03787753. DOI: 10.1016/j.jpowsour.2014.02.012.

[28] Long Lam and Pavol Bauer. “Practical Capacity Fading Model for Li-Ion Battery Cells in Electric Vehicles”. In: *IEEE Transactions on Power Electronics* 28.12 (Dec. 2013). Conference Name: IEEE Transactions on Power Electronics, pp. 5910–5918. ISSN: 1941-0107. DOI: 10.1109/TPEL.2012.2235083.

[29] Bolun Xu et al. “Modeling of Lithium-Ion Battery Degradation for Cell Life Assessment”. In: *IEEE Transactions on Smart Grid* 9.2 (Mar. 2018). Conference Name: IEEE Transactions on Smart Grid, pp. 1131–1140. ISSN: 1949-3061. DOI: 10.1109/TSG.2016.2578950.

[30] Joris de Hoog et al. “Combined cycling and calendar capacity fade modeling of a Nickel-Manganese-Cobalt Oxide Cell with real-life profile validation”. In: *Applied Energy* 200 (Aug. 2017), pp. 47–61. ISSN: 03062619. DOI: 10.1016/j.apenergy.2017.05.018.

[31] Noshin Omar et al. “Lithium iron phosphate based battery – Assessment of the aging parameters and development of cycle life model”. In: *Applied Energy* 113 (Jan. 2014), pp. 1575–1585. ISSN: 03062619. DOI: 10.1016/j.apenergy.2013.09.003.

[32] A. Maheshwari. *Modelling, aging and optimal operation of lithium-ion batteries*. OCLC: 8087222456. Technische Universiteit Eindhoven, Oct. 29, 2018. ISBN: 978-90-386-4607-7.

[33] Justin Purewal et al. “Degradation of lithium ion batteries employing graphite negatives and nickel–cobalt–manganese oxide + spinel manganese oxide positives: Part 2, chemical–mechanical degradation model”. In: *Journal of Power Sources* 272 (Dec. 2014), pp. 1154–1161. ISSN: 03787753. DOI: 10.1016/j.jpowsour.2014.07.028.

[34] Victor Agubra and Jeffrey Fergus. “Lithium Ion Battery Anode Aging Mechanisms”. In: *Materials* 6.4 (Apr. 2013). Number: 4 Publisher: Multidisciplinary Digital Publishing Institute, pp. 1310–1325. ISSN: 1996-1944. DOI: 10.3390/ma6041310.

[35] Vijay A. Sethuraman et al. “Surface structural disordering in graphite upon lithium intercalation/deintercalation”. In: *Journal of Power Sources* 195.11 (June 1, 2010), pp. 3655–3660. ISSN: 03787753. DOI: 10.1016/j.jpowsour.2009.12.034.

[36] Sophia Gantenbein et al. “Capacity Fade in Lithium-Ion Batteries and Cyclic Aging over Various State-of-Charge Ranges”. In: *Sustainability* 11.23 (Jan. 2019). Number: 23 Publisher: Multidisciplinary Digital Publishing Institute, p. 6697. ISSN: 2071-1050. DOI: 10.3390/su11236697.

[37] Jorn M. Reniers, Grietus Mulder, and David A. Howey. “Review and Performance Comparison of Mechanical-Chemical Degradation Models for Lithium-Ion Batteries”. In: *Journal of The Electrochemical Society* 166.14 (Sept. 19, 2019). Publisher: IOP Publishing, A3189. ISSN: 1945-7111. DOI: 10.1149/2.0281914jes.

[38] M. Scarfogliero et al. “Lithium-ion batteries for electric vehicles: A review on aging models for vehicle-to-grid services”. In: *2018 International Conference of Electrical and Electronic Technologies for Automotive*. 2018 International Conference of Electrical and Electronic Technologies for Automotive. July 2018, pp. 1–6. DOI: 10.23919/EETA.2018.8493211.

[39] Kailong Liu et al. “An evaluation study of different modelling techniques for calendar ageing prediction of lithium-ion batteries”. In: *Renewable and Sustainable Energy Reviews* 131 (Oct. 2020), p. 110017. ISSN: 13640321. DOI: 10.1016/j.rser.2020.110017.

[40] Mehdi Jafari, Khalid Khan, and Lucia Gauchia. “Deterministic models of Li-ion battery aging: It is a matter of scale”. In: *Journal of Energy Storage* 20 (Dec. 2018), pp. 67–77. ISSN: 2352152X. DOI: 10.1016/j.est.2018.09.002.

[41] Anthony Barré et al. “A review on lithium-ion battery ageing mechanisms and estimations for automotive applications”. In: *Journal of Power Sources* 241 (Nov. 2013), pp. 680–689. ISSN: 03787753. DOI: 10.1016/j.jpowsour.2013.05.040.

[42] S. Nejad, D.T. Gladwin, and D.A. Stone. “A systematic review of lumped-parameter equivalent circuit models for real-time estimation of lithium-ion battery states”. In: *Journal of Power Sources* 316 (June 2016), pp. 183–196. ISSN: 03787753. DOI: 10.1016/j.jpowsour.2016.03.042.

[43] Ruifeng Zhang et al. “A Study on the Open Circuit Voltage and State of Charge Characterization of High Capacity Lithium-Ion Battery Under Different Temperature”. In: *Energies* 11.9 (Sept. 2018). Number: 9 Publisher: Multidisciplinary Digital Publishing Institute, p. 2408. ISSN: 1996-1073. DOI: 10.3390/en11092408.

[44] John Wang et al. “Degradation of lithium ion batteries employing graphite negatives and nickel–cobalt–manganese oxide + spinel manganese oxide positives: Part 1, aging mechanisms and life estimation”. In: *Journal of Power Sources* 269 (Dec. 2014), pp. 937–948. ISSN: 03787753. DOI: 10.1016/j.jpowsour.2014.07.030.

[45] Issam Baghdadi et al. “Lithium battery aging model based on Dakin’s degradation approach”. In: *Journal of Power Sources* 325 (Sept. 2016), pp. 273–285. ISSN: 03787753. DOI: 10.1016/j.jpowsour.2016.06.036.

[46] You-Jin Lee et al. “Cycle life modeling and the capacity fading mechanisms in a graphite/LiNi0.6Co0.2Mn0.2O2 cell”. In: *Journal of Applied Electrochemistry* 45.5 (May 2015), pp. 419–426. ISSN: 0021-891X, 1572-8838. DOI: 10.1007/s10800-015-0811-6.

[47] Maciej Swierczynski et al. “Lifetime Estimation of the Nanophosphate $\hboxLiFePO_4\hbox/C$ Battery Chemistry Used in Fully Electric Vehicles”. In: *IEEE Transactions on Industry Applications* 51.4 (July 2015). Conference Name: IEEE Transactions on Industry Applications, pp. 3453–3461. ISSN: 1939-9367. DOI: 10.1109/TIA.2015.2405500.

[48] M. Schimpe et al. “Comprehensive Modeling of Temperature-Dependent Degradation Mechanisms in Lithium Iron Phosphate Batteries”. In: *Journal of The Electrochemical Society* 165.2 (2018), A181–A193. ISSN: 0013-4651, 1945-7111. DOI: 10.1149/2.1181714jes.

[49] Martin Petit, Eric Prada, and Valérie Sauvant-Moynot. “Development of an empirical aging model for Li-ion batteries and application to assess the impact of Vehicle-to-Grid strategies on battery lifetime”. In: *Applied Energy* 172 (June 2016), pp. 398–407. ISSN: 03062619. DOI: 10.1016/j.apenergy.2016.03.119.

[50] Yung-Li Lee and Tana Tjhung. “Rainflow Cycle Counting Techniques”. In: *Metal Fatigue Analysis Handbook*. Elsevier, 2012, pp. 89–114. ISBN: 978-0-12-385204-5. DOI: 10.1016/B978-0-12-385204-5.00003-3.

[51] *WebPlotDigitizer - Copyright 2010-2022 Ankit Rohatgi*. URL: https://apps.automeris.io/wpd/.

[52] Arnaud Delaille et al. “SIMCAL Project: calendar aging results obtained on a panel of 6 commercial Li-ion cells”. In: *224ème Electrochemical Energy Summit de l’Electrochemical Society*. San Fransisco, United States, Oct. 2013, 1 p.

[53] I Bloom et al. “An accelerated calendar and cycle life study of Li-ion cells”. In: *Journal of Power Sources* 101.2 (Oct. 2001), pp. 238–247. ISSN: 03787753. DOI: 10.1016/S0378-7753(01)00783-2.

[54] John Wang et al. “Cycle-life model for graphite-LiFePO4 cells”. In: *Journal of Power Sources* 196.8 (Apr. 2011), pp. 3942–3948. ISSN: 03787753. DOI: 10.1016/j.jpowsour.2010.11.134.